



OPEN ACCESS

EDITED BY Geeta Rai, Banaras Hindu University, India

REVIEWED BY
Yuxin Dong,
Tianjin Medical University General
Hospital, China
Guiying Hou,
The 2nd Affiliated Hospital of Harbin Medical
University, China

*CORRESPONDENCE
Wenlin Huang
Mhnzzhwl@hotmail.com

RECEIVED 29 May 2025
ACCEPTED 17 September 2025
PUBLISHED 02 October 2025

CITATION

Cheng T, Xu Y, Liu Z, Wang Y, Zhang Z and Huang W (2025) Multi-omics analysis reveals neutrophil heterogeneity and key molecular drivers in sepsis-associated acute kidney injury. Front. Immunol. 16:1637692. doi: 10.3389/fimmu.2025.1637692

COPYRIGHT

© 2025 Cheng, Xu, Liu, Wang, Zhang and Huang. This is an open-access article distributed under the terms of the Creative Commons Attribution License (CC BY). The use, distribution or reproduction in other forums is permitted, provided the original author(s) and the copyright owner(s) are credited and that the original publication in this journal is cited, in accordance with accepted academic practice. No use, distribution or reproduction is permitted which does not comply with these terms.

Multi-omics analysis reveals neutrophil heterogeneity and key molecular drivers in sepsisassociated acute kidney injury

Tianle Cheng¹, Yong Xu¹, Ziwei Liu¹, Yanchen Wang², Ze Zhang³ and Wenlin Huang^{1*}

¹Department of Urology, Zhuzhou Hospital Affiliated to Xiangya School of Medicine, Central South University, Zhuzhou, Hunan, China, ²Pharmacy Department, Zhuzhou Hospital Affiliated to Xiangya School of Medicine, Central South University, Zhuzhou, Hunan, China, ³Department of Urology, The Third People's Hospital of Datong, Datong, Shanxi, China

Sepsis-associated acute kidney injury is a critical condition driven by immune dysregulation, particularly involving neutrophils, yet their heterogeneity and molecular contributions remain underexplored. This study employed a multiomics approach, integrating single-cell and bulk RNA sequencing from 21 sepsis samples and Escherichia coli-induced sepsis datasets, alongside bioinformatics, machine learning, and experimental validation in a rat model and human peripheral blood. We identified four neutrophil subtypes-proinflammatory, anti-inflammatory, mature, and immature-revealing a significant increase in pro-inflammatory neutrophils in sepsis (40.53% versus 4.19% in controls) and a decrease in anti-inflammatory neutrophils (18.43% versus 27.04%). Four hub genes, peptidyl arginine deiminase 4, caspase 4, complement receptor 1, and mitogen-activated protein kinase 14, were pinpointed as key drivers, with peptidyl arginine deiminase 4 mediating neutrophil extracellular trap formation and exacerbating renal damage. In a rat model, peptidyl arginine deiminase 4 knockdown reduced trap formation and alleviated kidney injury (p-value less than 0.01). Human samples confirmed elevated gene expression in sepsis (p-value less than 0.05). These findings highlight neutrophil heterogeneity and molecular mechanisms in sepsis, with potential implications for sepsis-associated acute kidney injury (SAKI), proposing novel biomarkers and therapeutic targets for precision medicine.

KEYWORDS

sepsis, acute kidney injury, neutrophil heterogeneity, neutrophil extracellular traps (NETs), multi-omics, peptidyl arginine deiminase 4, biomarkers

1 Introduction

Sepsis, characterized by life-threatening organ dysfunction due to a dysregulated host response to infection, presents a complex pathophysiology with heterogeneous onset and prognosis, prompting extensive research (1). Acute kidney injury is the most frequent organ damage in sepsis, particularly in intensive care settings, with an incidence reaching 57.3 (2). In urosepsis, kidney damage occurs through multiple pathways: bacterial toxins such as lipopolysaccharides directly impair renal tubular epithelial and endothelial cells, systemic inflammation disrupts hemodynamic stability leading to reduced renal perfusion (3), and local bacterial effects within the urinary tract exacerbate injury (4-6). This interplay creates a vicious cycle, where urosepsis triggers acute kidney injury, and worsening kidney function intensifies systemic inflammation and toxin accumulation (5, 6). Consequently, early infection control is critical to reduce renal burden, while preserved kidney function is vital for successful sepsis management (2, 6). Clinically, timely relief of urinary tract obstruction in urosepsis can effectively reverse systemic inflammation and kidney damage.

Neutrophils, the most abundant white blood cells, are pivotal in the early immune response to sepsis, serving as a routine marker for assessing inflammation severity and prognosis (7). However, neutrophils are a heterogeneous population, with distinct subtypes emerging during granulopoiesis and exhibiting diverse roles across tissues and developmental stages (7). Recent studies have identified various neutrophil subpopulations, highlighting their divergent functions in inflammation (8, 9). Despite these advances, the specific roles of neutrophil heterogeneity in sepsis-associated acute kidney injury, particularly in urosepsis, remain underexplored. Single-cell transcriptomics offers a powerful approach to dissect this heterogeneity, uncover novel biomarkers, and elucidate immune interactions, yet its application in sepsis-related kidney injury is limited.

Given the lack of systematic studies on neutrophil heterogeneity and molecular mechanisms in sepsis-associated acute kidney injury, this study was necessary to address this gap. We aimed to characterize neutrophil subtypes and identify key molecular drivers in sepsis-associated kidney injury, focusing on Escherichia coli-induced sepsis. Notably, while the datasets used in this study represent general sepsis cohorts without explicit SAKI diagnostic criteria (e.g., KDIGO stages based on serum creatinine or urine output), our findings on neutrophil heterogeneity provide insights into sepsis-induced immune dysregulation that may contribute to SAKI. By integrating single-cell and bulk RNA sequencing with experimental validation, we sought to uncover novel biomarkers and therapeutic targets, contributing to precision medicine strategies for sepsis management and improving outcomes in patients with sepsis-associated acute kidney injury.

2 Materials and methods

2.1 Single-cell data collection

Two single-cell transcriptome datasets related to sepsis were obtained from the Gene Expression Omnibus (GEO) database

(https://www.ncbi.nlm.nih.gov), specifically GSE175453 (which includes 9 samples) and GSE167363 (which includes 12 samples). In total, 21 single-cell transcriptomic samples were utilized for various analyses, including cell annotation, identification of neutrophils and their subtypes, pseudo-time series analysis, and the identification of differentially expressed genes in neutrophils from healthy individuals compared to those from sepsis patients. These datasets, capturing peripheral blood mononuclear cells (PBMCs) and leukocytes from sepsis patients, reflect systemic immune responses potentially relevant to organ dysfunction, including SAKI, though they lack explicit kidney-specific clinical annotations based on KDIGO criteria (e.g., serum creatinine or urine output).

2.2 Data quality control and batch removal

Cell tags, genes, and expression matrices were obtained directly from the GEO database, and the Seurat v4 package (10) was utilized to process the data. The filtering criteria applied to the pooled samples included: $300 < nFeature_RNA < 2000$, $nCount_RNA < 40000$, percent.mt (ratio of mitochondrial genes) < 30, and log10GenesPerUMI > 0.85.

2.3 Dimensionality reduction, annotation, differential expression

The Seurat pipeline was utilized to reduce the dimensionality of the combined cell data. First, principal component analysis (PCA) was conducted and visualized, followed by the creation of an elbow plot to identify the most significant principal components. The harmony algorithm (11) was then employed to address batch effects among various samples. After that, Dimensionality reduction was performed on the selected principal components (PCs) using both UMAP and t-SNE. Subsequently, cluster plots were generated to determine the optimal resolution parameter for partitioning cells into biologically distinct clusters.

The dataset was annotated into different cell types, such as T lymphocytes, B lymphocytes, neutrophils, and plasma cells, using the CellMarker2 database. Visualization was enhanced through bubble plots of marker genes and UMAP annotation plots.

Differential expression analysis was carried out using the FindAllMarkers function, aiming to identify differentially expressed genes within the same group across different clusters, as well as those within the same cluster but across different groups. Genes were selected as differentially expressed if they met the criteria of $|\log FC| > 0.25$ and a P-value < 0.05.

2.4 Pseudo-time analysis

Pseudo-time trajectory analysis was conducted using the Monocle package (12). Highly variable genes were selected based on an average expression threshold (>0.1) and ranked within the

top 2000 by coefficient of variation. Dimensionality reduction was performed using the DDRTree algorithm (13), and cellular trajectories were visualized through scatter plots generated by the built-in plot_cell_trajectory function. Genes were partitioned into two distinct clusters based on their pseudo-temporal expression patterns. Differential gene expression along the pseudo-time axis was visualized using the plot_pseudotime_heatmap function. Gene Ontology (GO) enrichment analysis for temporally dynamic pathways was subsequently performed with the clusterProfiler package (14), employing a significance threshold of p < 0.05 and false discovery rate (FDR) < 0.25.

2.5 Cell-cell communication analysis

Cell-cell communication analysis was performed on annotated cell subpopulations using the CellChat package (15). Ligand-receptor interactions were predicted based on a predefined signaling pathway database. Key communication patterns were visualized through three types of diagrams: (1) Cell-cell interaction networks representing connections between cell clusters; (2) Incoming signaling heatmaps showing receptor activity in target cell types; (3) Outgoing signaling heatmaps displaying ligand expression in source cell types. All visualizations were generated using default settings of the CellChat package.

2.6 Metabolic pathway analysis

Metabolic pathway activities across cell types were analyzed using the scMetabolism package (16). Heatmaps were generated to visualize pathway activity differences.

2.7 Bulk RNA-seg data collection

Publicly available datasets were retrieved from the Gene Expression Omnibus (GEO) database The following datasets were included:

- Escherichia coli-induced sepsis dataset (GSE237960): Due to
 the scarcity of urosepsis-specific datasets in public repositories,
 this dataset was selected as a surrogate based on the clinical
 relevance of *E. coli* as the predominant pathogen in urinary
 tract infections. The GSE237960 dataset was selected as a
 surrogate for urosepsis, given that E. coli is the predominant
 pathogen in urosepsis (70-80% of cases) and shares immune
 mechanisms such as neutrophil activation, NET formation,
 and cytokine responses with general E. coli sepsis (17–19).
 Whole blood RNAseq data of 4 patients with Escherichia coli
 sepsis (experimental group) and 4 normal people (Control
 group) were included; Platform: Affymetrix Human Genome
 U133 Plus 2.0 Array; Purpose: Identification of differentially
 expressed genes (DEGs) and exploratory data mining.
- 2. Sepsis training/validation dataset (GSE185263): Platform: Affymetrix Human Gene 1.0 ST Array (GPL6244); Purpose:

- Construction of a support vector machine (SVM) model, immune cell infiltration analysis, and preliminary validation of candidate genes.
- 3. External validation dataset (GSE243217): Platform: Affymetrix Human Gene 1.0 ST Array (GPL6244); Purpose: Independent validation of diagnostic performance for hub genes.
- 4. NETF pathway gene set: A curated list of 132 genes associated with neutrophil extracellular traps (NETs) formation, a process where neutrophils release chromatin fibers to immobilize pathogens during infection or inflammation. The data source is the KEGG database (https://www.kegg.jp/, accession: hsa04613).

2.8 Bulk RNA-seq data preprocessing

Raw transcriptomic data were downloaded from the GEO database using the GEO query package (20). Platform-specific annotation files were utilized to map probes to gene symbols. Expression matrices were normalized via the RMA algorithm (21), including background correction, quantile normalization, and probe summarization. For genes with multiple probes, expression values were averaged to generate gene-level measurements.

2.9 Differential expression analysis

Differentially expressed genes (DEGs) were identified in the *E. coli*-induced sepsis dataset using the limma package (21). Linear models comparing sepsis patients and controls were fitted after variance-stabilizing normalization. Statistical significance was defined as $|\log_2 FC| > 0.5$ and p < 0.05, with FDR correction applied to control false discoveries (FDR < 0.1).

2.10 Functional enrichment analysis (GO/KEGG)

GO and KEGG analyses were performed using the clusterProfiler package (14, 22) Gene sets included pseudotime-associated DEGs (Section 2.4) and *E. coli*-sepsis DEGs (Section 2.8). Significant terms (FDR < 0.05) were visualized as lollipop charts (top 9 KEGG pathways) and dot plots (top 3 GO terms per category).

2.11 Venn diagram, machine learning (SVM), and single-gene ROC analysis

The CNSKnowall Cloud Platform (https://www.cnsknowall.com/veen) was utilized to generate a Venn diagram illustrating the overlap between NETF genes, neutrophil differential genes, and differential genes identified through Bulk-RNAseq. This analysis enabled the identification of neutrophil-urosepsis differential genes. A linear SVM model was trained on 70% of GSE185263 and

validated on 30%, with diagnostic performance assessed by ROC curves using the pROC package (23). Hub genes with AUC > 0.7 were prioritized.

2.12 Immune infiltration analysis

To characterize the immune microenvironment in urosepsis, samples from the GSE185263 dataset were stratified into normal and sepsis groups. Immune cell infiltration profiles were quantified using the xCell algorithm (24), which estimates the abundance of 64 immune and stromal cell types based on gene expression signatures. The proportions of infiltrating immune cells were visualized through stacked bar plots generated with the ggplot2 package (version 3.4.0).

To identify differential immune infiltration between high-risk and low-risk subgroups (defined by the hub gene expression signature), the Wilcoxon rank-sum test was applied with a significance threshold of p < 0.05. Statistically significant cell types were further visualized using violin plots to display distribution differences. Associations between hub genes (PADI4, CR1, MAPK14, CASP4) and immune cell infiltration were analyzed via Spearman correlation and represented as lollipop plots, where the dot size and color intensity reflected correlation coefficients (ρ) and significance levels, respectively.

Additionally, the interplay between hub genes and immune checkpoint molecules (e.g., PD-L1, TIM-3, CTLA-4) was explored through heatmaps, with hierarchical clustering applied to both rows (genes) and columns (checkpoint genes). Immune cell types showing significant co-enrichment patterns were highlighted in enrichment bubble plots, where bubble size indicated the -log10(*p*-value) and color denoted enrichment scores.

2.13 Gene set enrichment analysis of hub genes

To investigate the biological pathways associated with hub genes in the disease, Gene Set Enrichment Analysis (GSEA) was performed using the training dataset from GSE185263. The "c2.cp.kegg.v7.0.symbols.gmt" gene set from the Molecular Signatures Database (MSigDB) was used as the reference gene set. First, Spearman correlation coefficients between each hub gene and all other genes in the dataset were calculated using the R package "psych" (version 2.5.3) (25). For each hub gene, a ranked gene list was generated by sorting all genes in descending order based on their correlation coefficients. Subsequently, GSEA was conducted using the R package "clusterProfiler" (version 3.8) to explore the potential functional roles of the hub genes (14). Analysis parameters were set at p < 0.05, FDR < 0.25, and |NES| > 1, with hub gene enrichment results visualized and reported.

2.14 Consensus clustering analysis

In this study, data preprocessing and consensus clustering were performed to identify the optimal clustering approach. Initially, a specific gene set, denoted as gene_Consensus, was selected from the raw dataset. Each gene (row) was then subjected to median centering by subtracting its row-specific median. For the consensus clustering analysis, Pearson correlation was employed as the distance metric, with partitioning around medoids (PAM) as the clustering algorithm. The analysis parameters were set as follows: a maximum cluster number of 6, 1000 iterations, a subsampling rate of 80% of the samples, inclusion of all features, use of complete observations for correlation calculations, and a fixed random seed of 814 to ensure reproducibility. The optimal number of clusters (k) was determined by incrementally increasing k from 2 to 6, with k=2 identified as the optimal clustering solution based on clustering stability.

2.15 Subcellular localization analysis

To investigate the subcellular distribution of hub genes, subcellular localization analysis was performed using the GeneCards database (https://www.genecards.org/). The localization of these genes to specific organelles, along with their confidence scores, was visualized as bar plots using the R package "ggplot2".

2.16 DGIdb drug interaction analysis

To explore existing drugs associated with the identified hub genes, drug-gene interaction data were retrieved from the DGIdb database (https://www.dgidb.org/). The relationships between hub genes and related drugs, including their interaction scores, were visualized as bar plots using the R package "ggplot2".

2.17 Establishment of the sepsis rat's model

The experiment utilized male Wistar rats (8–10 weeks old, 160–200 g; SLAC Laboratory Animal Co., Ltd., Shanghai, China), housed at 22 ° C with 50% humidity and a 12:12 h light-dark cycle, with ad libitum access to standard chow and water. Rats were acclimated to the environment for at least one week prior to experimentation. All procedures were approved by the Institutional Animal Care and Use Committee (IACUC) and complied with national and international guidelines for animal experimentation. Rats were randomly assigned to three groups (n=3 per group): Sham group (laparotomy without cecal ligation or puncture), CLP group (cecal ligation and double puncture with a 20-gauge needle to induce sepsis), and CLP + sh-PADI4 group (CLP surgery followed by tail vein injection of 1×10⁹ TU PADI4targeting shRNA adenovirus). The CLP model was performed under aseptic conditions. Rats were anesthetized with 2.5% isoflurane, underwent midline laparotomy, and the cecum was ligated below the ileocecal valve and punctured twice with a 20-gauge needle, with a small amount of fecal matter extruded before abdominal closure. The Sham group underwent cecal exposure without ligation or puncture. Adenovirus was administered via slow tail vein injection, with all interventions conducted under anesthesia. Rats were fasted for 8-12 hours pre-surgery, recovered in a warm environment post-surgery, and

monitored closely, adhering to predefined humane endpoints to minimize suffering. At 48 hours post-CLP, rats were euthanized under deep anesthesia, blood was collected via cardiac puncture, and serum was stored at -80°C. Both kidneys were harvested—one fixed in 10% neutral-buffered formalin or 4% paraformaldehyde for histological and immunofluorescence analysis, the other snap-frozen in liquid nitrogen and stored at -80°C for molecular assays. Aseptic techniques were maintained throughout, and sepsis-related tissues were disposed of according to biosafety protocols. The animal study was approved by the Institutional Animal Care and Use Committee of The Second Xiangya Hospital, Central South University (Approval No: 2022711).

2.18 Western blotting analysis

Kidney tissues from the CLP and Sham groups were homogenized in RIPA buffer containing protease inhibitors and centrifuged at 12,000 \times g for 15 min at 4°C to extract proteins. Protein concentrations were determined using the BCA method. Thirty micrograms of protein were mixed with loading buffer, heated at 95°C for 5 min, separated by 10% SDS-PAGE, and transferred to a PVDF membrane. The membrane was blocked with 5% non-fat milk for 1 h, incubated overnight at 4°C with primary antibodies against PADI4 (1:1000, Abcam) and β-actin (1:5000, Sigma-Aldrich), washed with TBST, and incubated with HRP-conjugated secondary antibodies (anti-rabbit 1:5000, anti-mouse 1:10000) for 1h. After further TBST washes, bands were visualized using ECL detection. Band intensities were quantified with ImageJ, and PADI4 expression was normalized to β-actin.

2.19 Immunofluorescence staining

Kidney tissues from experimental groups were fixed in 4% paraformaldehyde at 4°C for 24–48 h, dehydrated, and embedded in paraffin. Sections (4–5 μm) were cut, mounted on adhesive slides, and baked at 60°C for 30 min. After deparaffinization in xylene and rehydration through a graded ethanol series, antigen retrieval was performed in citrate buffer (pH 6.0) at 95°C for 15 min. Sections were cooled, washed with PBS, and blocked with 5% goat serum in PBS for 30 min at room temperature. Sections were then incubated with anticitH3 antibody (1:200, Abcam) overnight at 4°C, washed with PBS, and incubated with Alexa Fluor 488-conjugated anti-rabbit secondary antibody (1:500, Thermo Fisher Scientific) for 1 h at room temperature in the dark. Nuclei were counterstained with DAPI for

5 min, and slides were mounted with anti-fade medium. Images were captured using a fluorescence microscope and quantified for citH3-positive cells using ImageJ software.

2.20 Hematoxylin and eosin staining

Kidney tissues from experimental groups were fixed in 10% neutral-buffered formalin at room temperature for 24–48 h, dehydrated through a graded ethanol series, cleared in xylene, and embedded in paraffin. Sections (4–5 μm) were cut using a microtome, mounted on adhesive slides, and baked at 60°C for 30 min. Sections were deparaffinized in xylene, rehydrated through decreasing ethanol concentrations, and stained with hematoxylin for 5 min. After rinsing in tap water, sections were differentiated in 1% acid alcohol, blued in ammonia water, and counterstained with eosin for 1 min. Sections were dehydrated, cleared in xylene, and mounted with a coverslip using mounting medium. Images were captured using a bright-field microscope, and histopathological changes were evaluated.

2.21 Quantitative real-time PCR analysis

Peripheral blood samples were collected from 5 sepsis patients and 5 healthy controls. And the study of these samples was approved by the Ethics Committee of Zhuzhou Hospital Affiliated to Xiangya School of Medicine, Central South University (Approval No: 2020175-01). Total RNA was extracted from whole blood using TRIzol reagent (Invitrogen, USA) per the manufacturer's instructions. cDNA was synthesized from 1 μ g total RNA using the PrimeScript RT reagent kit (Takara, Japan). Quantitative real-time PCR was performed on a CFX96 system (Bio-Rad, USA) with SYBR Green premix (Takara, Japan). Expression of PADI4, CASP4, CR1, and MAPK14 was measured, normalized to β -actin (primer sequences in Table 1). Relative gene expression was calculated using the 2^- $\Delta\Delta$ Ct method.

2.22 Statistical analysis

All analyses were executed utilizing R programming language (v 4.2.2). The Wilcoxon test was harnessed to contrast differences, employing a statistical threshold of p < 0.05.

¹ Material and Methods section can be placed in any of the following ways.

TABLE 1 Primer sequences for qRT-PCR.

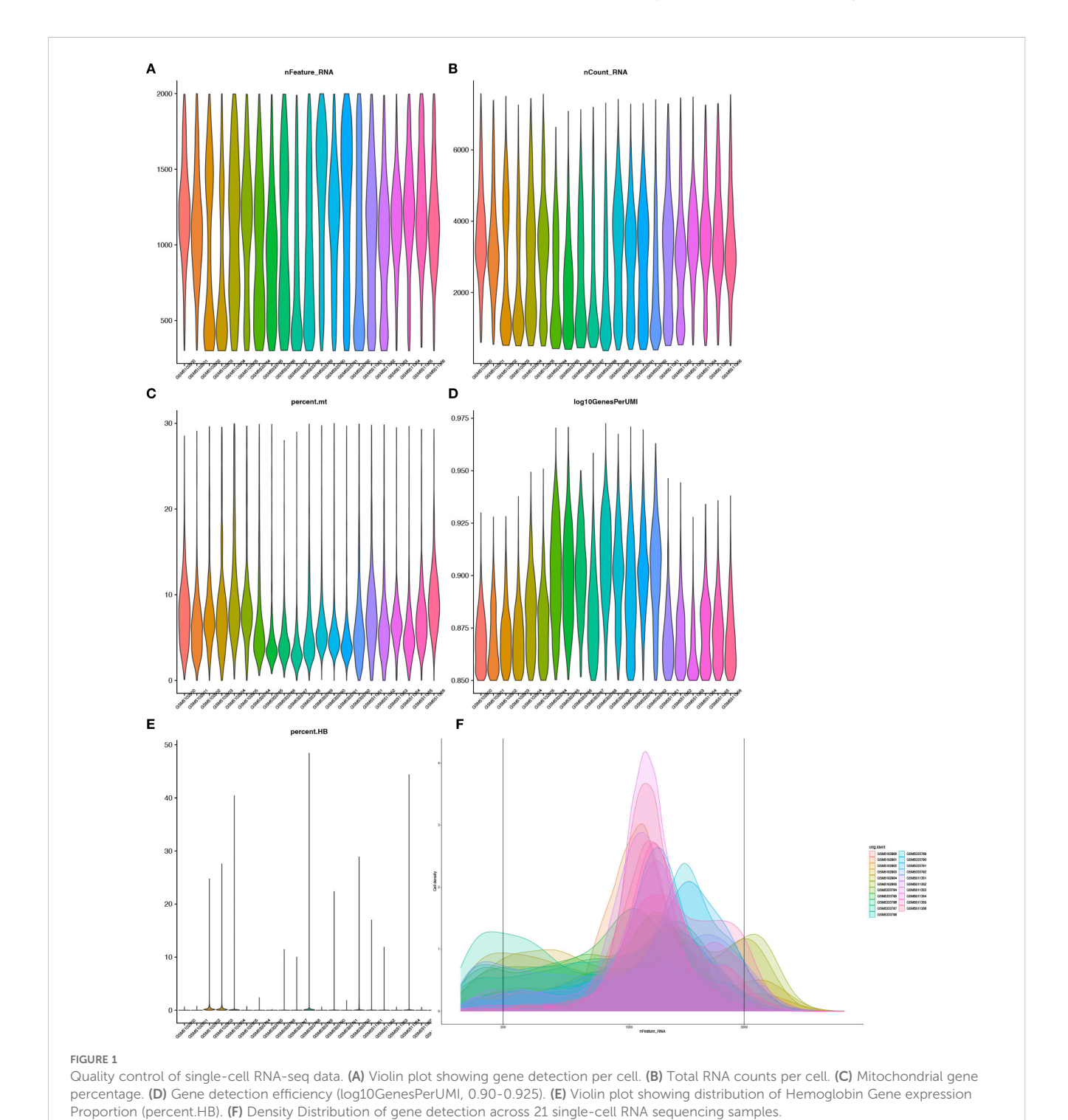
Gene	Forward primer	Reverse primer
PADI4	CAGGGGACATTGATCCGTGTG	GGGAGGCGTTGATGCTGAA
CASP4	TCTGCGGAACTGTGCATGATG	TGTGTGATGAAGATAGAGCCCAT
CR1	CACGAAGCCGCCAATTTGTC	CCCACTTGATCGTCATTGCTG
MAPK14	TCAGTCCATCATTCATGCGAAA	AACGTCCAACAGACCAATCAC
β-actin	CATGTACGTTGCTATCCAGGC	CTCCTTAATGTCACGCACGAT

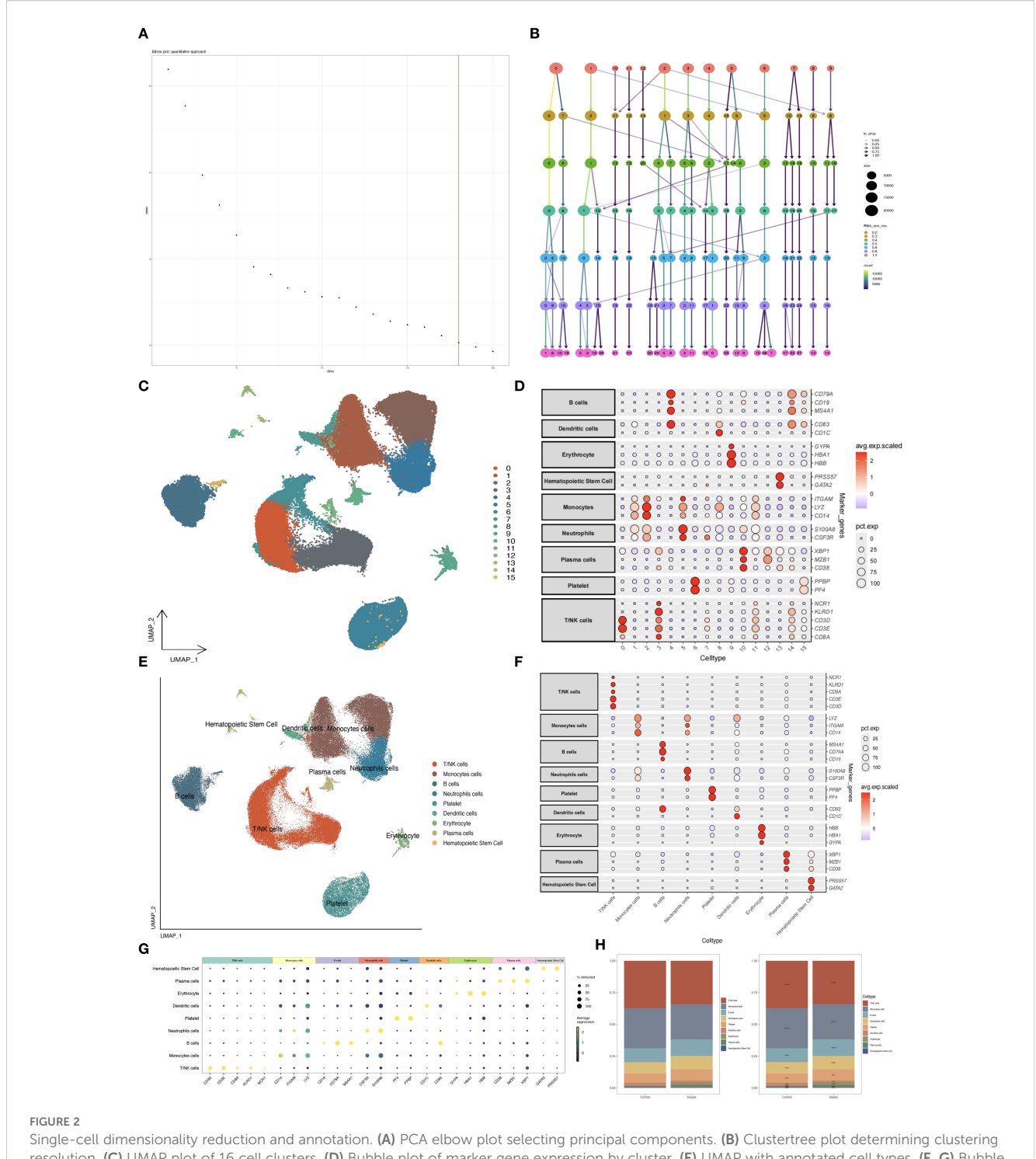
3 Results

3.1 Data filtering and cell population identification

21 single-cell transcriptome samples were retrieved from the GEO database (GSE175453, 9 samples; GSE167363, 12 samples). Quality control was performed using Seurat v4 with the following criteria: 300 < nFeature_RNA < 2000, nCount_RNA < 40000, percent.mt < 30, and

log10GenesPerUMI > 0.85. This confirmed a high-quality dataset (Figures 1A–F). Batch effects were corrected using the Harmony algorithm, followed by principal component analysis (PCA) to select significant components (Figure 2A). UMAP dimensionality reduction was applied with an optimal resolution determined by cluster tree analysis (Figure 2B), clustering cells into 16 groups with distinct marker gene expression profiles (Figure 2D). These were annotated as 9 distinct cell types, including B cells, T/NK cells, monocytes, and neutrophils (Figures 2C, E). In the sepsis group, the proportion of



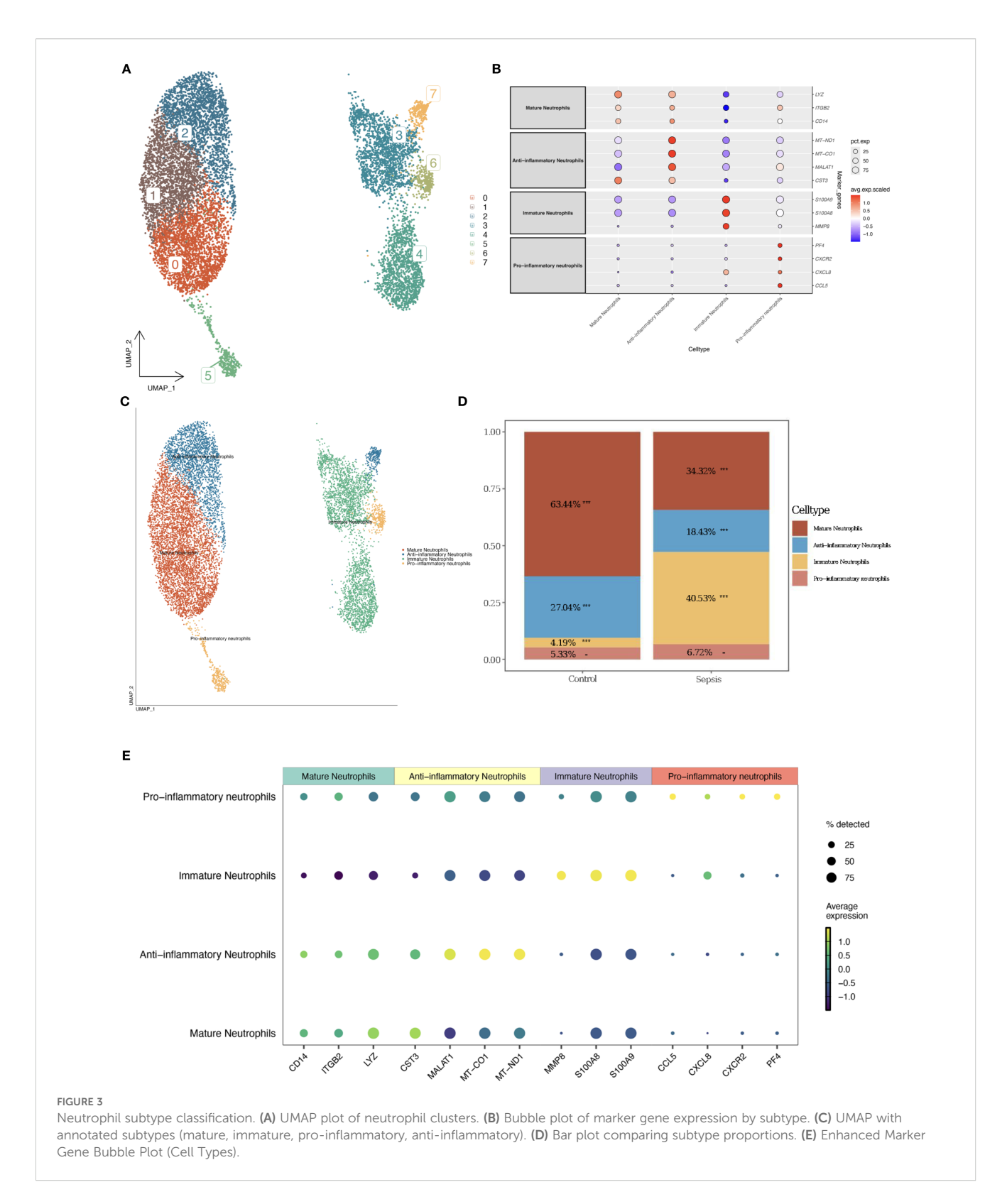


resolution. (C) UMAP plot of 16 cell clusters. (D) Bubble plot of marker gene expression by cluster. (E) UMAP with annotated cell types. (F, G) Bubble plots of marker genes by cell type. (H) Bar plot comparing cell type proportions.

neutrophils was significantly elevated (10.63% vs. 8.94% in the healthy group), while T/NK cells showed a slight reduction (34% vs. 37%), and monocytes remained consistent (27%, Figure 2H). Marker gene analysis validated cell identities, with neutrophils highly expressing S100A8 and CSF3R, and T/NK cells expressing CD3E and KLRD1 (Figures 2F, G), providing a foundation for subsequent neutrophil-focused analyses.

3.2 Neutrophil subtype classification

Neutrophils were subdivided into 8 clusters using UMAP, which were further categorized into four subtypes based on immune-related and metabolic gene expression profiles: mature neutrophils, immature neutrophils, anti-inflammatory neutrophils, and pro-inflammatory neutrophils (Figures 3A, C). Anti-inflammatory neutrophils, defined



by elevated MT-ND1, MT-CO1, MALAT1, and CST3, were more prevalent in the control group (27.04% vs. 18.43% in sepsis, Figure 3D), while pro-inflammatory neutrophils, distinguished by PF4, CXCR2, CXCL8, and CCL5, exhibited a slight increase in sepsis (6.72% vs. 5.33% in controls, Figure 3D), suggesting an intensified inflammatory state. Anti-inflammatory neutrophils were identified by high

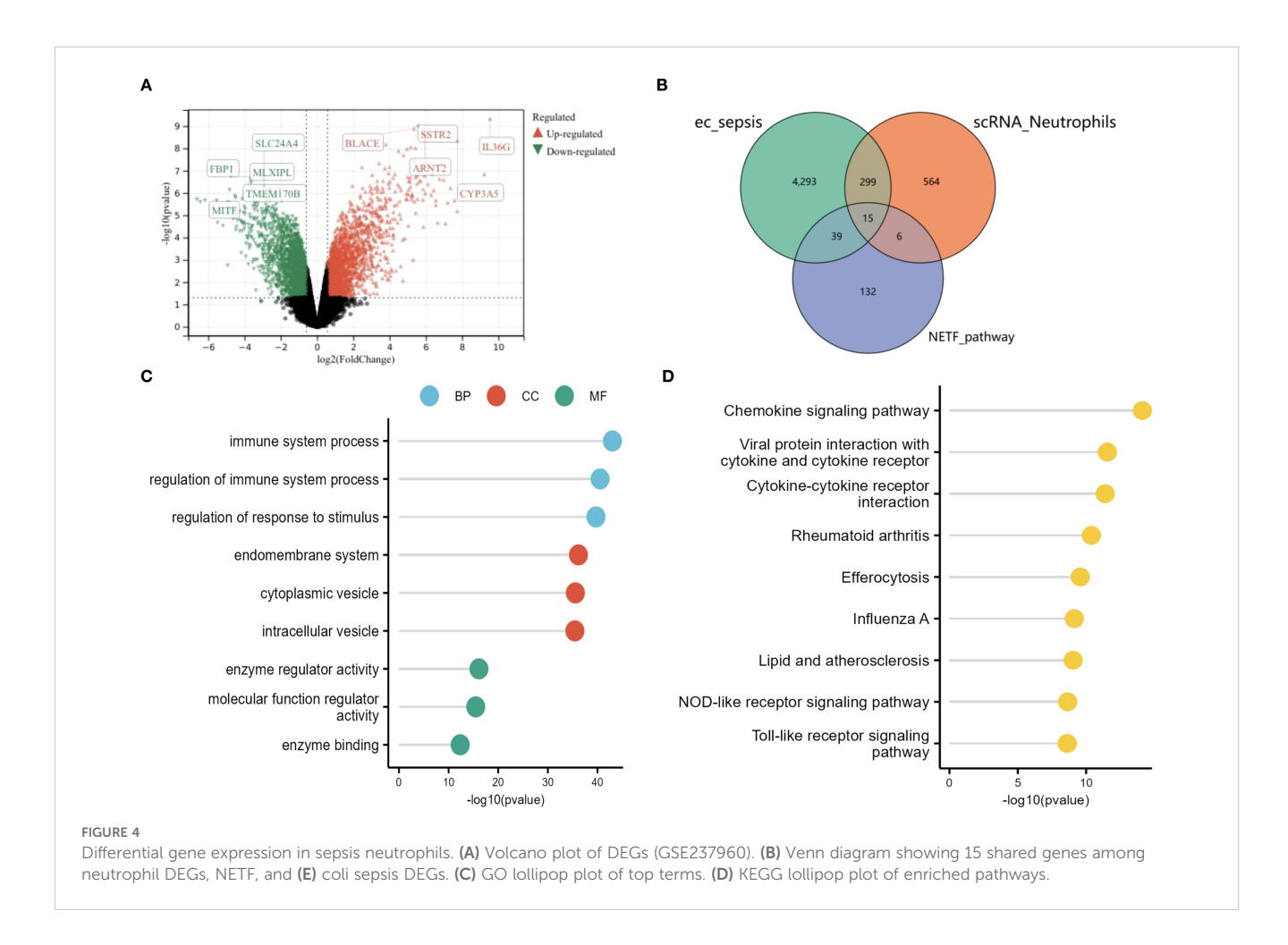
expression of MT-ND1, MT-CO1, MALAT1, and CST3, which are associated with mitochondrial homeostasis and inflammation resolution (26–28). Pro-inflammatory neutrophils were characterized by elevated PF4, CXCR2, CXCL8, and CCL5, promoting chemotaxis and inflammatory amplification in sepsis (29–33). Minimal cross-expression of marker genes across subtypes validated the robustness

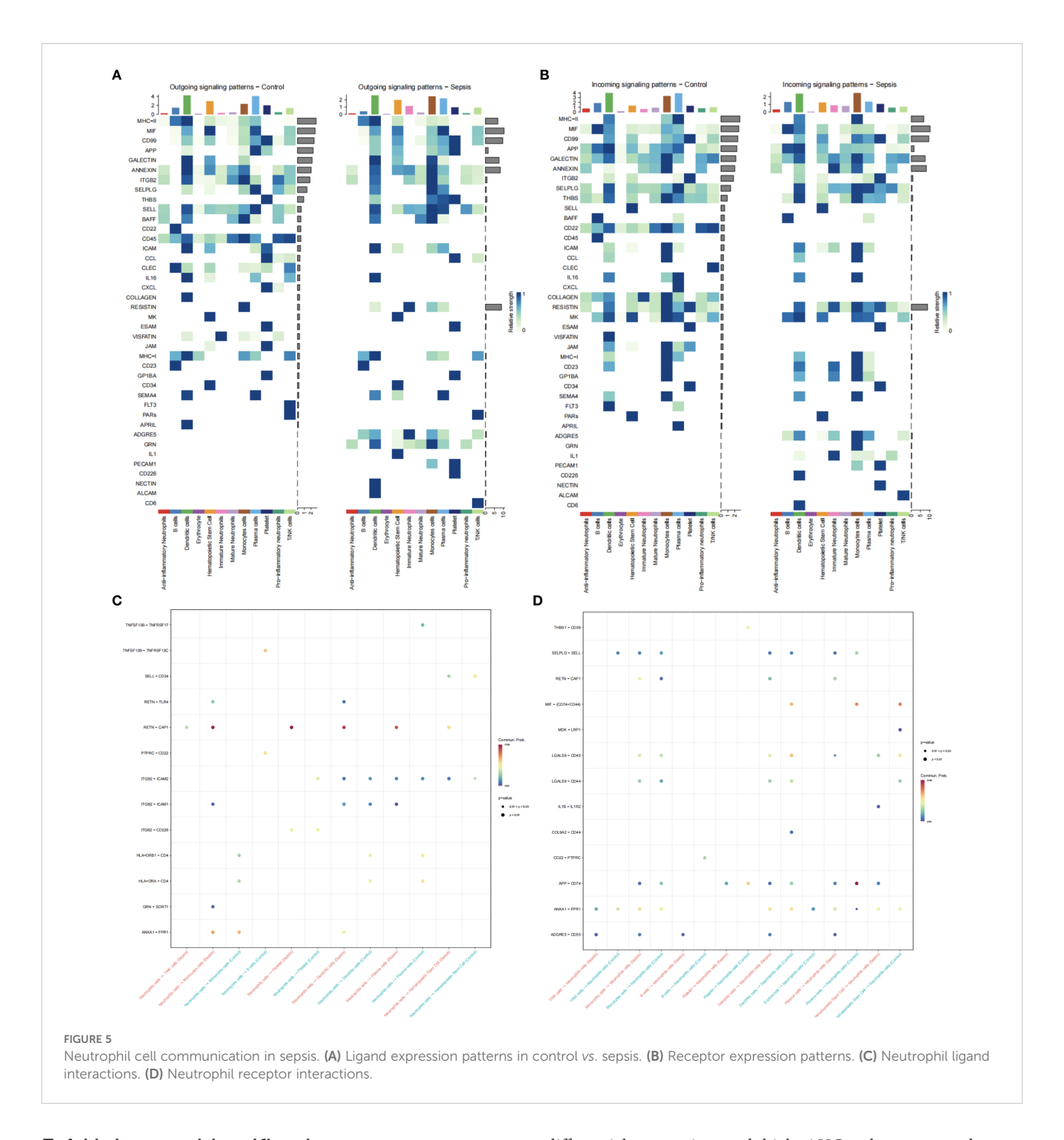
of this classification (Figures 3B, E). The substantial increase in immature neutrophils in the sepsis group (40.53% vs. 4.19% in controls, Figure 3D) underscored their mobilization during acute inflammation. The decrease in anti-inflammatory neutrophils (18.43% vs. 27.04%) and the slight rise in pro-inflammatory neutrophils (6.72% vs. 5.33%) further indicated an immune imbalance, potentially contributing to the exacerbated inflammation in sepsis.

3.3 Functional and dynamic analysis of neutrophils

Differential expression analysis (GSE237960, Escherichia coliinduced sepsis) identified 4646 differentially expressed genes (DEGs), with 2312 upregulated and 2334 downregulated (Figure 4A). To narrow down key neutrophil-specific genes, DEGs were intersected across neutrophil pseudotime, neutrophil extracellular trap formation (NETF) pathways, and E. coli-induced sepsis, resulting in 15 shared genes (Figure 4B). These DEGs were enriched in chemokine signaling, cytokine-cytokine receptor interaction, and Toll-like receptor pathways (Figures 4C, D), reflecting enhanced immune and inflammatory responses in sepsis. Cell communication analysis revealed increased IL-1 signaling (e.g., IL1A-FPR1, IL1B-FPR1) in the sepsis group,

suggesting a stronger pro-inflammatory response and potential therapeutic relevance of IL-1 receptor antagonists (e.g., Anakinra). Suppression of HLA-DRB1-CD4 signaling (Figures 5A-D) indicated impaired antigen presentation, which may contribute to adaptive immune dysregulation. In the control group, metabolic activities such as glycolysis and fatty acid metabolism were predominant in mature neutrophils (Figures 6A, B). In the sepsis group, we observed a significant upregulation of biotin and lipoic acid metabolism in mature neutrophils (Figure 6B)—a pattern also observed in immature and proinflammatory subtypes—suggesting metabolic reprogramming under inflammatory conditions. Pseudotime analysis revealed a continuous trajectory of neutrophil states (Figure 7A), with distinct state distributions reflecting developmental progression (Figure 7B). A shift toward an early pro-inflammatory state was observed in sepsis neutrophils compared to controls (Figure 7C), with immature subtypes enriched in early stages and mature and anti-inflammatory subtypes in later stages (Figure 7D). The expression patterns of the 15 shared genes along the pseudotime axis further highlighted their dynamic regulation, with genes like PADI4 showing elevated expression in early proinflammatory stages (Figure 7E). Gene clustering revealed two expression patterns: Cluster 1 (low early, high late) enriched in immune processes, and Cluster 2 (high early, low late) enriched in protein synthesis (Figures 8A-C), illustrating dynamic neutrophil regulation in sepsis.





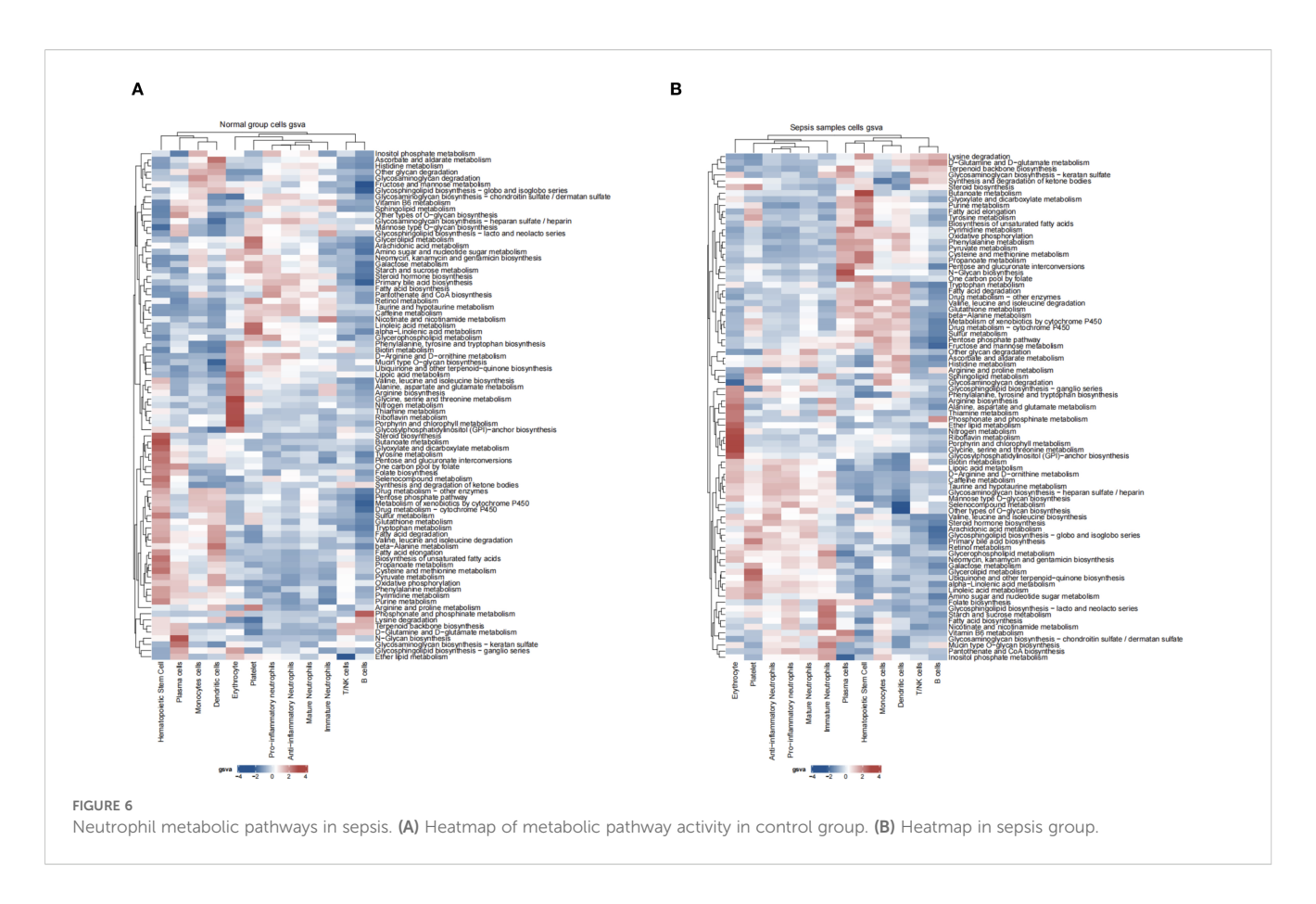
3.4 Hub gene identification

To identify hub genes linked to neutrophil function in sepsis, differential gene expression data were integrated and validated externally using a support vector machine (SVM) model. An SVM model trained on 70% of the GSE185263 dataset identified PADI4, CASP4, CR1, and MAPK14 as significant feature genes (Figure 9A). Internal validation yielded an AUC of 0.9372, with only 2 misclassified samples (Figures 9B, C). External validation using GSE243217 confirmed high AUC values: PADI4 (92.4%), CASP4 (90.6%), CR1 (97.3%), and MAPK14 (93.9%) (Figures 9D, E). The consistent

differential expression and high AUC values across datasets underscored their reliability as hub genes in sepsis.

3.5 Functional analysis and therapeutic potential of hub genes

Gene set enrichment analysis (GSEA) indicated that all four hub genes were enriched in immune and inflammation-related pathways, suggesting synergistic roles in sepsis immune regulation. Specifically, PADI4 was enriched in Pathogenic Escherichia coli Infection (NES =

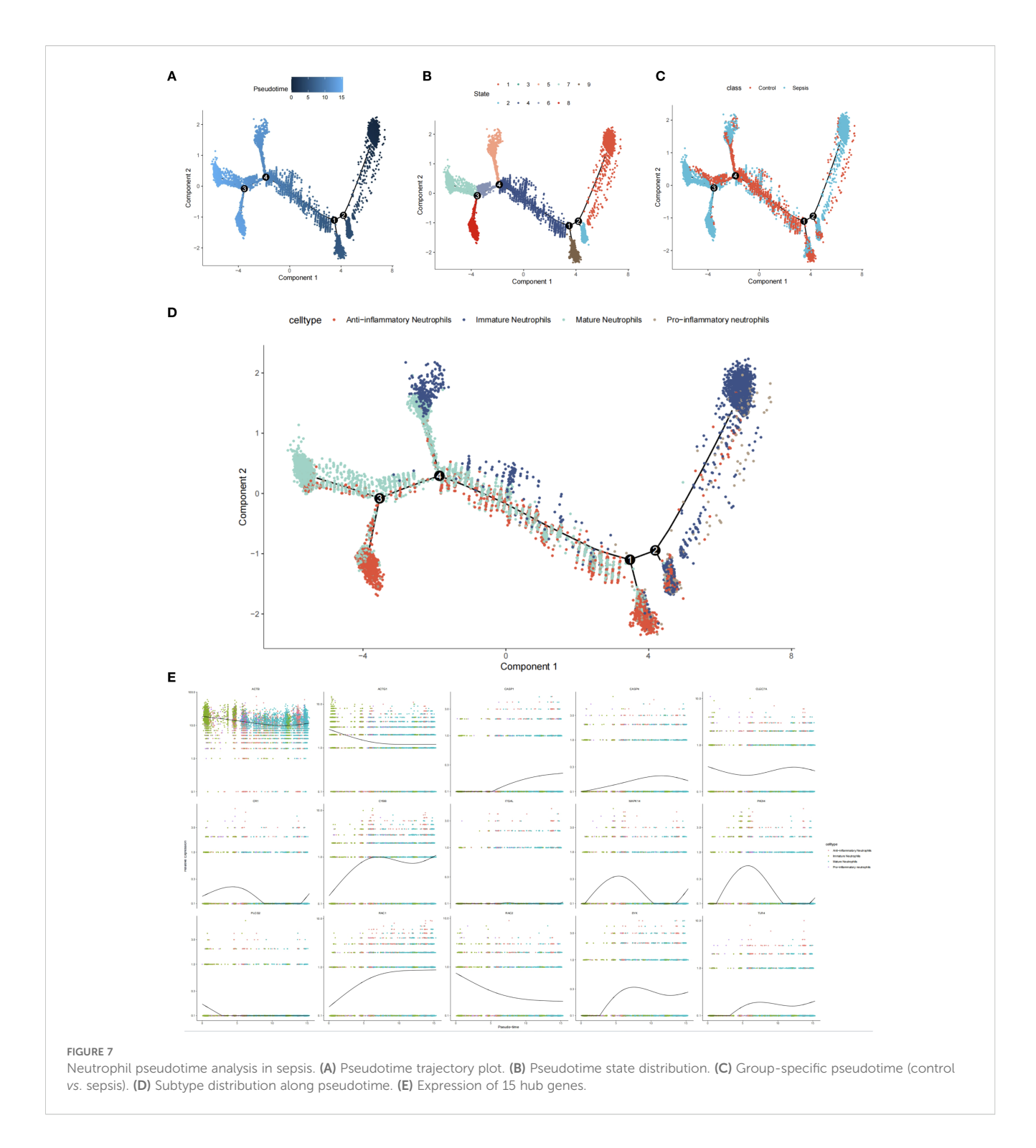


1.62, p = 8.56e-07, FDR = 1.22e-05) and Fc Gamma R-Mediated Phagocytosis (NES = 1.62, p = 9.31e-10, FDR = 1.47e-07, Figure 10A). CASP4 showed enrichment in Leishmania Infection (NES = 1.70, p = 1.03e-08, FDR = 2.80e-07), B Cell Receptor Signaling Pathway (NES = 1.69, p = 1.04e-09, FDR = 3.88e-08), and Proteasome (NES = 1.67, p = 1.10e-06, FDR = 1.14e-05, Figure 10B). CR1 and MAPK14 were enriched in B Cell Receptor Signaling and Renal Cell Carcinoma pathways (Figures 10C, D). Subcellular localization analysis revealed PADI4 primarily in the cytosol and nucleus, CASP4 in the endoplasmic reticulum and cytosol, CR1 in the extracellular space and plasma membrane, and MAPK14 in the cytosol, extracellular space, and nucleus (Figures 11A-D), supporting their functional diversity. Drug-gene interaction analysis suggested potential therapeutic candidates, including uric acid for PADI4, emricasan for CASP4, and RO-3201195 for MAPK14 (Figures 12A-D), offering directions for targeted sepsis therapies. Consistent with this prediction, preclinical studies demonstrated that febuxostat treatment lowered tissue urate levels and significantly reduced citH3 expression in mice (34), indicating suppression of PAD4-dependent NETosis in vivo.

3.6 Immune microenvironment and clustering analysis

Immune microenvironment analysis revealed significantly increased neutrophil infiltration (P<0.001) and reduced T cell infiltration (e.g., CD4+ memory T cells, P<0.001) in the sepsis

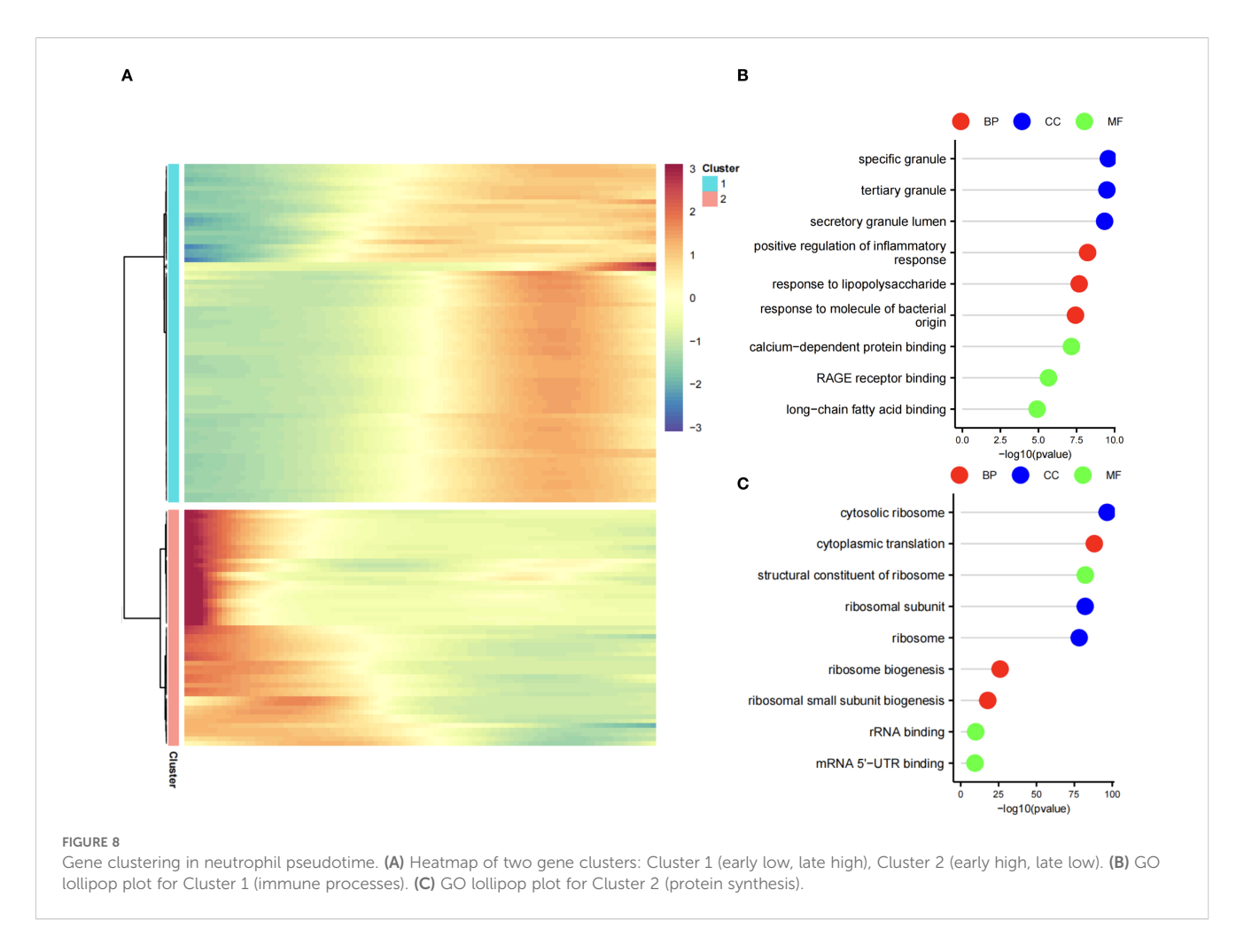
group (Figures 13A, C), with a strong negative correlation between neutrophils and T cells (P<0.001, Figure 13B). PADI4, CASP4, CR1, and MAPK14 were positively correlated with neutrophil infiltration (P<0.001) and negatively correlated with T cell infiltration (P<0.001, Figure 13D), and positively associated with immune checkpoint genes (CD24, CD47, P<0.01, Figure 13E), suggesting immunosuppressive mechanisms. The increased neutrophil infiltration and decreased T cell presence indicated an imbalance between innate and adaptive immunity in sepsis, potentially linked to disease severity. To corroborate these xCell-derived profiles, CIBERSORT analysis was applied to the same bulk RNA-seq data, estimating proportions of 22 immune cell types. Consistent with xCell findings, it confirmed significantly elevated neutrophil fractions in the sepsis group (P < 0.001; Supplementary Figures 1A, C) and reduced T cell subtypes, such as CD4 memory activated T cells. Neutrophils and T cells showed a strong negative correlation (Supplementary Figure 1B), while the hub genes exhibited positive correlations with neutrophil infiltration (r = 0.3-0.7, Supplementary Figure 1C). These genes were also positively associated with immune checkpoint molecules (Supplementary Figure 1E), reinforcing the immunosuppressive microenvironment. Consensus clustering divided patients into two clusters: Cluster A exhibited lower PADI4 and CASP4 expression and higher CR1 and MAPK14 expression (Figures 14A-D), highlighting molecular heterogeneity. However, survival differences between clusters were not statistically significant (p=0.7594), possibly due to limited sample size, necessitating further clinical validation.



3.7 Validation of hub genes in sepsis

To investigate the role of hub genes in sepsis-associated kidney injury, we employed a cecal ligation and puncture (CLP) model to induce sepsis in mice, followed by extraction of kidney tissues for *in vitro* experimental analyses to assess the expression differences of PADI4. Western blot (WB) analysis revealed a significant upregulation of PADI4 expression in the kidney tissues of the CLP group compared to the sham-operated group, with quantitative

analysis (normalized to β -actin) confirming a markedly higher relative expression level (p < 0.001, Figures 15A, B). The full uncropped Western Blot images are provided in Supplementary Figure S2. Immunofluorescence (IF) staining further demonstrated a pronounced increase in the red fluorescence signal of citrullinated histone H3 (citH3, a marker of neutrophil extracellular trap [NET] formation) in the kidney tissues of the CLP group, significantly exceeding that of the sham group (p < 0.001). Notably, knockdown of PADI4 resulted in reduced citH3 expression, suggesting a critical

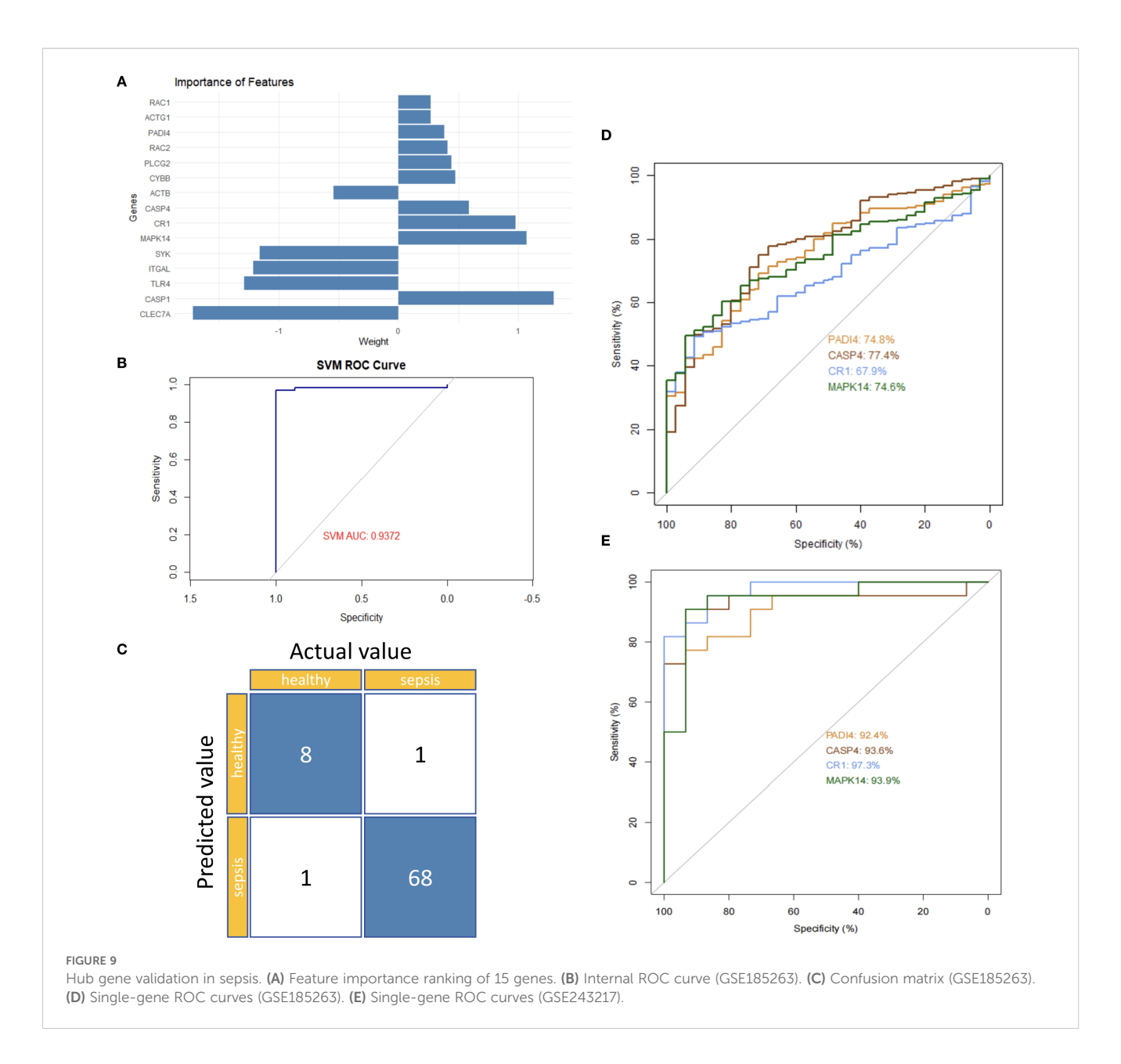


role for PADI4 in sepsis-induced NET formation (p < 0.001 compared to the CLP group, Figures 15C, D). Hematoxylin and eosin (H&E) staining revealed significant pathological changes in the kidney tissues of the CLP group, characterized by tubular dilation, expansion of the tubulointerstitial area, and inflammatory cell infiltration, consistent with the features of sepsis-induced acute kidney injury. The injury score was significantly higher in the CLP group than in the sham group (p < 0.001). However, PADI4 knockdown markedly attenuated these pathological changes (p < 0.01 compared to the CLP group, Figures 15E, F), indicating that PADI4 silencing significantly ameliorates sepsis-induced renal histopathological damage. Furthermore, we validated the elevated expression of the hub genes in the peripheral blood of patients with sepsis, consistent with our previous findings (compared to the control group, Figures 15G–J).

4 Discussion

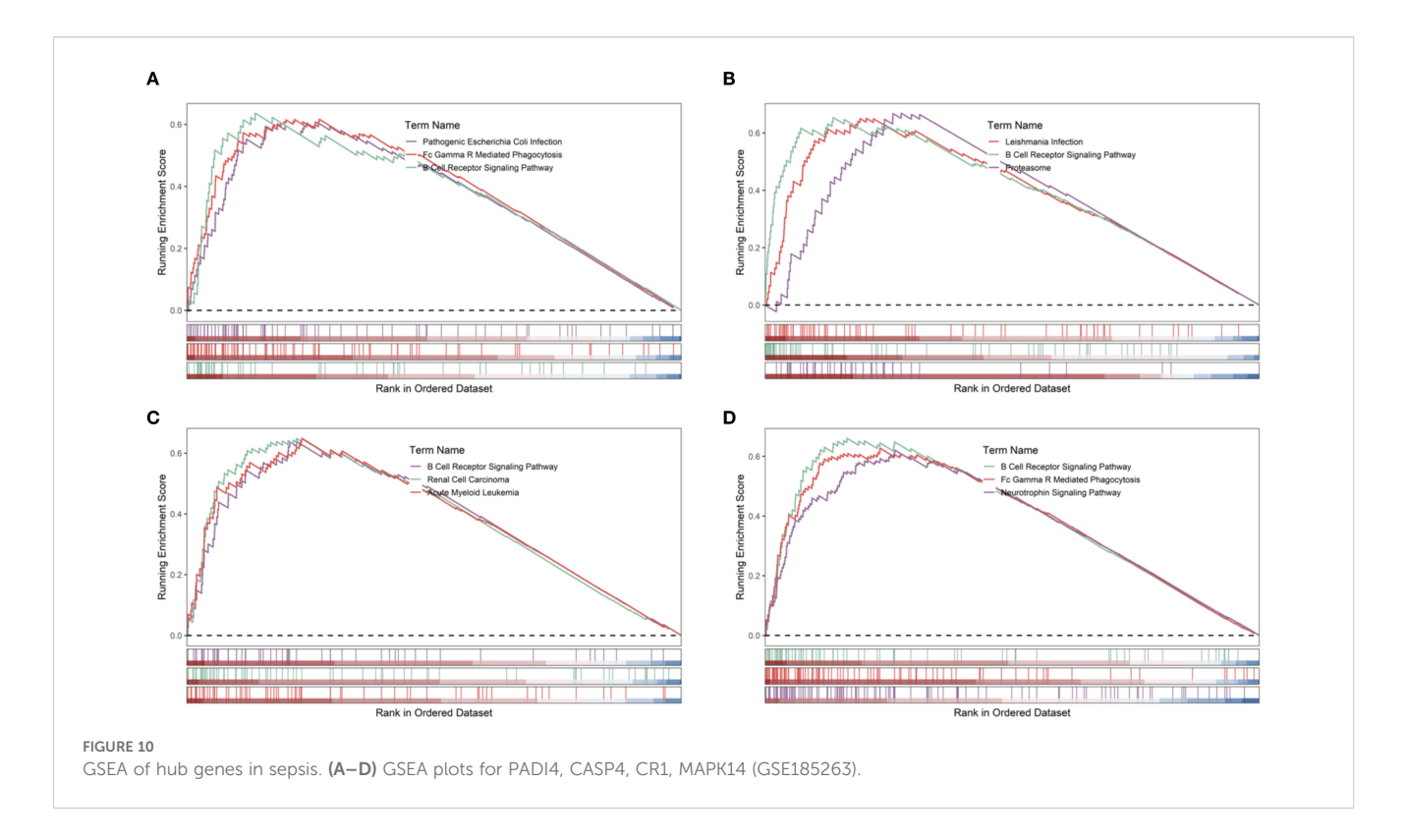
In this study, we identified four neutrophil subtypes, with the delineation of pro-inflammatory and anti-inflammatory subtypes representing a significant innovation. Pro-inflammatory neutrophils were characterized by genes such as PF4, CXCR2, CXCL8, and CCL5, which play critical roles in amplifying inflammation. These genes enhance inflammatory responses through chemotaxis, degranulation,

and reactive oxygen species production (29, 35). For instance, CXCL8 mediates a positive feedback loop via CXCR2, promoting neutrophil recruitment (32). This self-amplifying signaling pathway is particularly prominent in chronic lung diseases such as chronic obstructive pulmonary disease and bronchiectasis (36). As a chemokine, CCL5 effectively attracts neutrophils to sites of infection or injury, thereby augmenting immune and inflammatory responses (30, 31). During the acute phase of sepsis, Ccl5-positive macrophages exhibited the strongest interaction with neutrophils, predominantly through the CCL signaling pathway, suggesting that Ccl5-positive macrophages play a key role in neutrophil recruitment via CCL5-CCR1 pairing (33) 。In contrast, anti-inflammatory neutrophils were distinguished by high expression of MT-ND1, MT-CO1, MALAT1, and CST3, which are associated with mitochondrial function, inflammation resolution, and tissue protection. MT-ND1 and MT-CO1, core components of the mitochondrial electron transport chain (complexes I and IV, respectively), maintain mitochondrial membrane potential and energy metabolism balance, supporting normal neutrophil function. Mitochondria contribute to inflammation resolution by regulating neutrophil apoptosis, exerting an antiinflammatory effect (27). Studies have shown that inhibitors of complexes I and III, such as rotenone and antimycin A, significantly reduce neutrophil migration (26). The anti-inflammatory effect of MALAT1 is primarily mediated by its regulation of IL-10 expression.



In a Leishmania Donovani model, MALAT1 knockout mice exhibited reduced IL-10 expression in CD4-positive T cells, enhancing macrophage activation and pathogen clearance (28). CST3 exerts its effects mainly by inhibiting cysteine proteases, with studies demonstrating that high cystatin C concentrations significantly suppress spontaneous, fMLP-, and PMA-induced neutrophil respiratory bursts (37). In the sepsis group, the proportions of proinflammatory and immature neutrophils were significantly elevated (40.53% and 6.72% vs. 4.19% and 5.33% in controls), while antiinflammatory neutrophils decreased (18.43% vs. 27.04%), consistent with a shift toward an early pro-inflammatory state in pseudotime analysis. This suggests that neutrophils in the acute phase of sepsis predominantly adopt an early pro-inflammatory state, reflecting immune mobilization against infection. However, this imbalance may lead to uncontrolled inflammation, exacerbating damage to renal tubular epithelial and endothelial cells, which aligns with the high incidence of sepsis-associated acute kidney injury. These findings not only elucidate the role of neutrophil heterogeneity in immune dysregulation during urosepsis but also provide a foundation for developing strategies to suppress pro-inflammatory subtypes or enhance the reparative functions of anti-inflammatory subtypes.

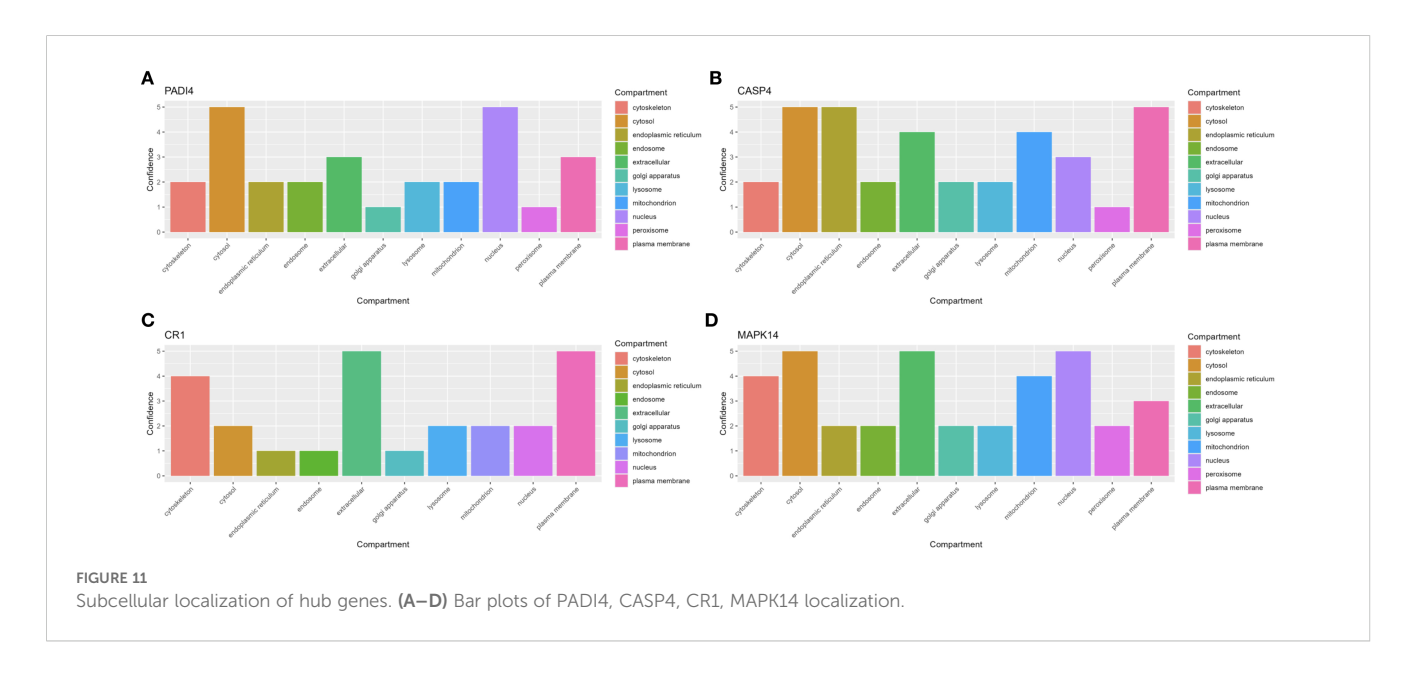
Beyond phenotypic heterogeneity, the dynamic regulation of neutrophil function is increasingly recognized as a critical determinant of sepsis outcomes. Recent studies have demonstrated that metabolic reprogramming and inflammatory signaling shape neutrophil effector functions, such as NET formation and cytokine release, thereby amplifying tissue injury in sepsis. Although direct mechanistic evidence in sepsis-associated AKI remains limited, related bioinformatics and network-based studies from other immune-inflammatory conditions have highlighted the interplay between metabolic pathways and immune cell heterogeneity (38–40). While these studies are not focused on sepsis per se, they provide

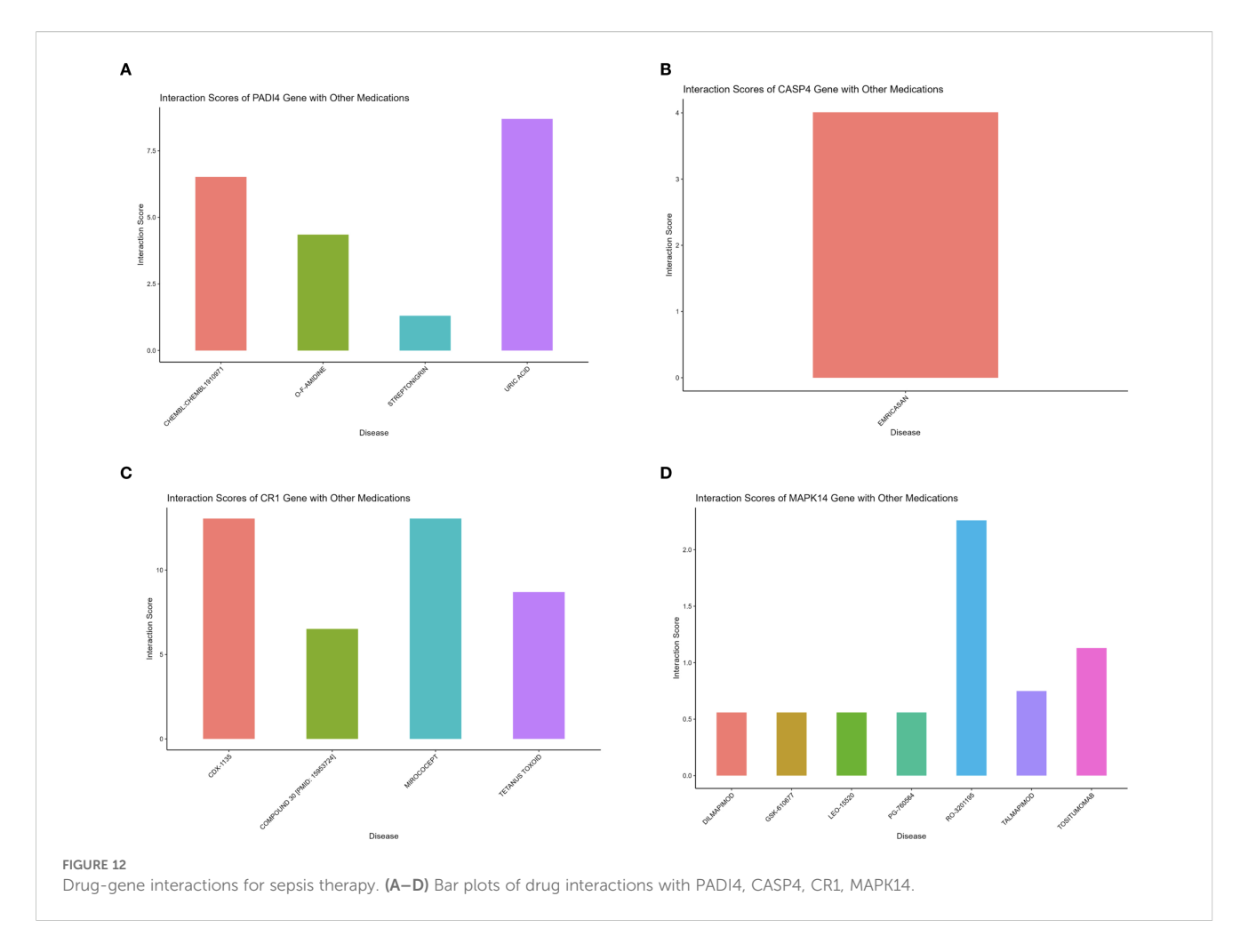


methodological and contextual insights supporting the concept that neutrophil subtypes may adopt distinct functional states under systemic inflammatory stress. Our findings extend this perspective by integrating multi-omics data with experimental validation, specifically linking PAD4-driven pro-inflammatory neutrophils to renal injury in sepsis.

Integrative analysis of single-cell and bulk RNA sequencing data, combined with machine learning, further identified PADI4, CASP4, CR1, and MAPK14 as hub genes in sepsis. These genes exhibited high expression in neutrophils and positively correlated with neutrophil infiltration, underscoring their significance in the

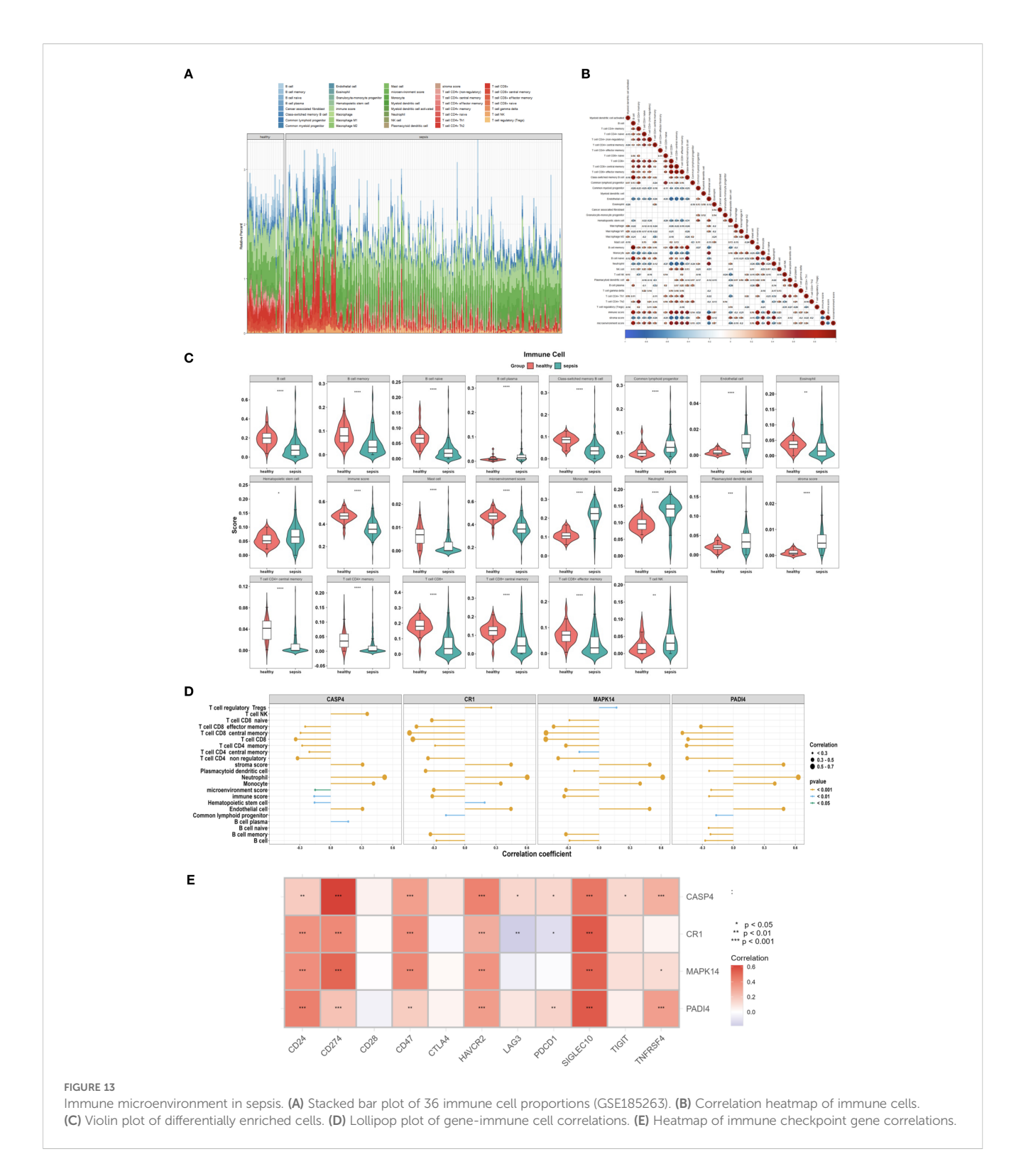
inflammatory response during sepsis. Neutrophil extracellular traps (NETs) have emerged as important players in sepsis. Although extracellular in nature, their components can directly injure renal tubular cells (41). Notably, urosepsis may differ immunologically from other sepsis types, yet NETs remain scarcely studied in this context. To address this gap, we focused on NETs-related genes and intersected them with E. coli-induced and neutrophil-associated gene sets. PADI4 plays a dual role in sepsis by mediating NETosis (neutrophil extracellular trap formation). On one hand, it contributes to infection defense by capturing pathogens such as Escherichia coli through NETs, a process involving the conversion



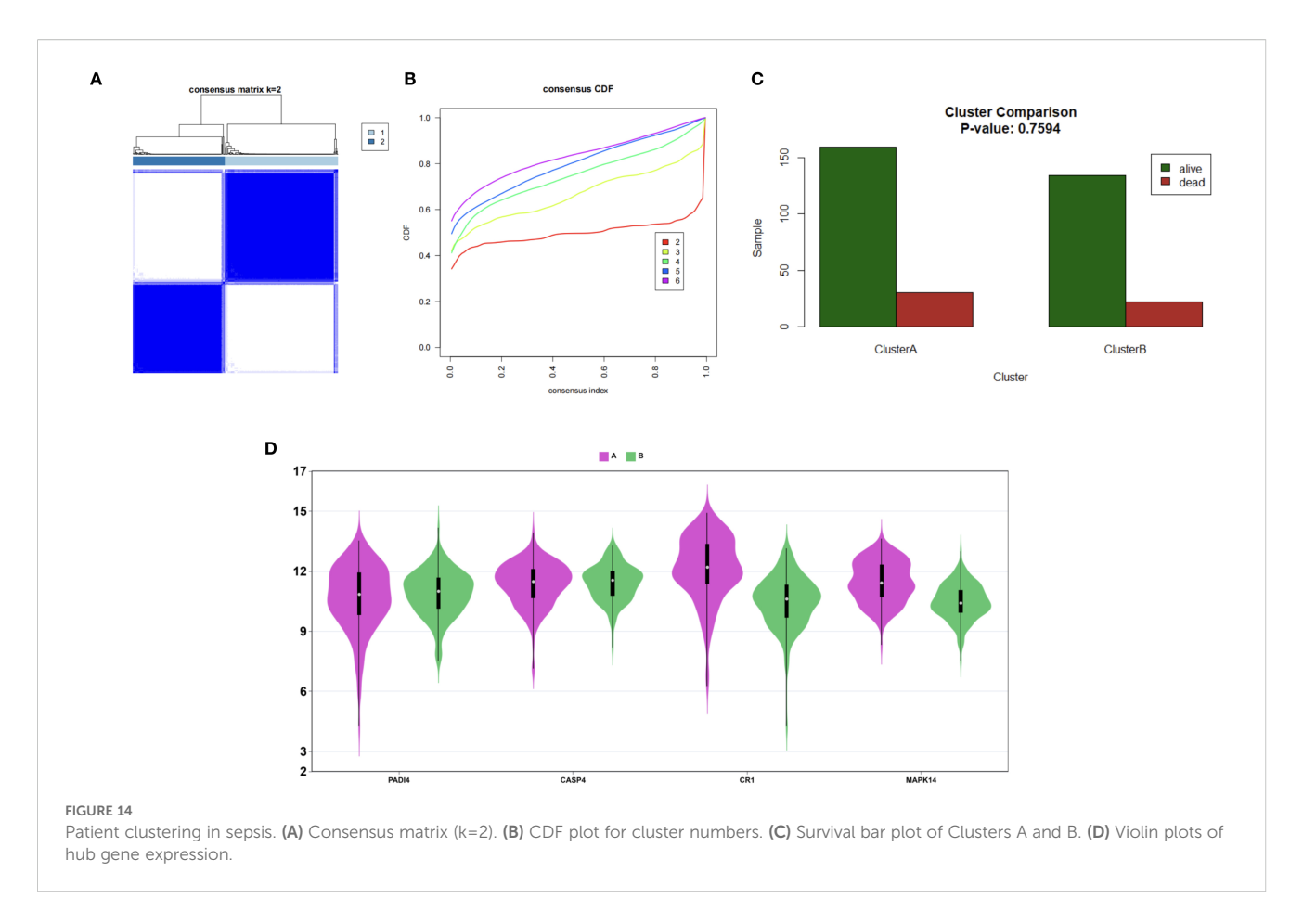


of arginine residues in histones to citrulline, significantly reducing histone positive charge (42, 43). This modification weakens the electrostatic interactions between positively charged histones and negatively charged DNA, leading to nucleosome destabilization and chromatin decondensation (44). Studies have shown that in PADI4deficient neutrophils, histone H3 citrullination is completely absent, and NETosis induced by PMA and LPS does not occur (45). Moreover, PADI4 inhibitors significantly block histone citrullination and NET release (46, 47). On the other hand, excessive NET release may exacerbate renal tissue damage. Gene set enrichment analysis revealed PADI4 enrichment in the Escherichia coli infection pathway (NES = 1.62, FDR = 1.22e-05), supporting its specific role in sepsis. The therapeutic implications of targeting PADI4 merit further consideration. Preclinical evidence supports that pharmacological inhibition of PADI4 with smallmolecule inhibitors, such as Cl-amidine (a pan-PAD inhibitor), significantly reduces renal ischemia/reperfusion-induced acute kidney injury, attenuates tubular inflammation, and decreases neutrophil infiltration in murine models (48, 49). Furthermore, specific PAD4 inhibition using GSK484 has demonstrated renal protection by reducing remote lung injury, NET formation, and histone H3 citrullination in acute kidney injury contexts (50). Although these inhibitors are not yet in clinical use, they provide a compelling proof-of-concept that PADI4 inhibition holds promise

as a therapeutic strategy for SAKI. CASP4 directly binds cytoplasmic lipopolysaccharide, particularly its active component lipid A, via its CARD domain, forming a multimeric complex that activates its enzymatic activity and induces pyroptosis (51). This process also triggers NLRP3 inflammasome assembly, promoting the release of IL-1\beta and IL-18, thereby amplifying the immune response (52)_a CR1 facilitates the clearance of immune complexes by binding C3b and C4b (53), preventing their deposition in vulnerable tissues such as the kidney and lungs (54), thus exhibiting anti-inflammatory and renoprotective potential. In systemic lupus erythematosus, studies have reported significantly reduced CR1 expression on erythrocytes and leukocytes, correlating with disease severity and renal involvement (55). MAPK14 is activated in response to various stimuli, including cytokines (e.g., TNF-α, IL-1β), oxidative stress, lipopolysaccharide, and viral infections (56). MAPK14 activates the downstream kinase MK2, which phosphorylates the RNA-binding protein TTP, preventing degradation of AU-rich element-containing mRNAs and stabilizing pro-inflammatory cytokine mRNAs such as TNF-α, IL-1β, and IL-6 (56, 57). This mechanism is particularly pronounced in macrophages and dendritic cells, promoting rapid inflammatory responses. MAPK14 also directly phosphorylates transcription factors such as NF-κB, ATF2, and MEF2, enhancing the transcriptional activity of pro-inflammatory genes (57).



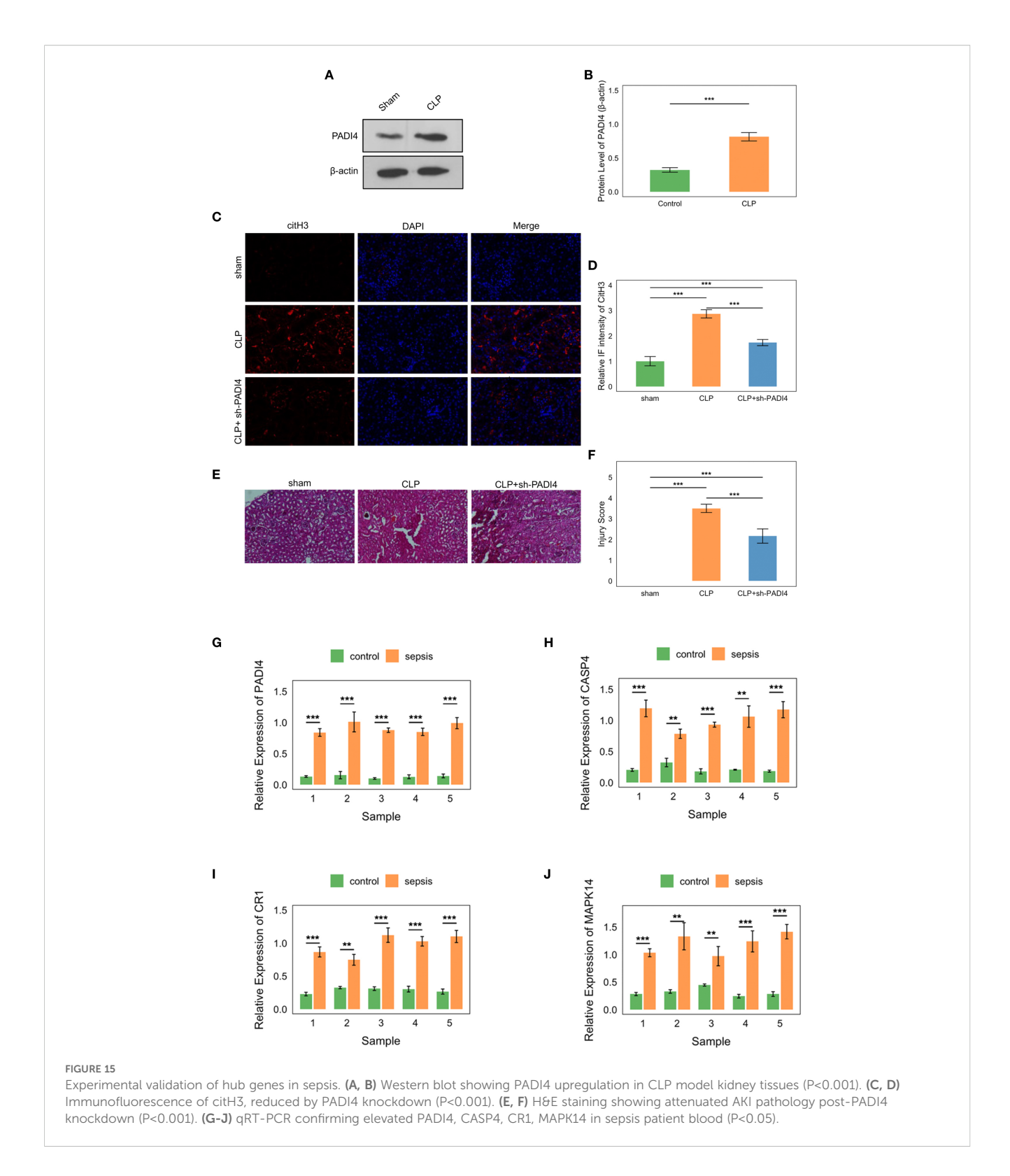
The pseudotime trajectory analysis revealed an early proinflammatory state shift in neutrophils during sepsis, characterized by increased expression of pro-inflammatory genes such as PADI4, which aligns with the significant rise in proinflammatory neutrophil proportions (40.53% in sepsis *vs.* 4.19% in controls, Figure 3D). This suggests that the early proinflammatory state may drive the expansion of pro-inflammatory neutrophils, potentially exacerbating renal damage through enhanced NETosis and inflammatory cascades. The concomitant decrease in anti-inflammatory neutrophils (18.43% in sepsis *vs.* 27.04% in controls) could reflect a shift in neutrophil maturation or functional reprogramming along the pseudotime axis, as supported by dynamic gene expression patterns (Figure 7E). Previous studies have demonstrated that pseudotime analysis can uncover cell state



transitions linked to subtype proportions, and our GSEA results (Figure 10) further indicate that pathways such as MAPK signaling (enriched for MAPK14) may underpin this transition.

Analysis of the immune microenvironment revealed significantly increased neutrophil infiltration and decreased T cell infiltration in the sepsis group, reflecting an imbalance between hyperactive innate immunity and suppressed adaptive immunity. This imbalance may exacerbate renal damage through excessive activation of pro-inflammatory neutrophils. The positive correlation between hub genes and immune checkpoint genes (CD24, CD47, HAVCR2; $\rho = 0.40$ -0.80, P < 0.01) suggests an immunosuppressive mechanism. Previous studies have shown that PD-L1 expression on neutrophils is upregulated during sepsis, potentially suppressing adaptive immunity via the PD-L1/PD-1 checkpoint (58), a phenomenon also observed in our study. This T cell suppression, driven by immune checkpoint activation, may have implications for secondary infections, a common complication in sepsis linked to immunoparalysis (59). Literature indicates that T cell dysfunction, particularly through PD-1/PD-L1 signaling (60), impairs pathogen clearance and increases susceptibility to opportunistic infections such as Gram-negative bacteria (61). The observed suppression, potentially influenced by neutrophil-driven inflammation and hub gene activities (e.g., PADI4, MAPK14), could contribute to this risk. CD24 interacts with SIGLEC10 to inhibit macrophage phagocytosis (62). Li et al. suggested that the CD24-SIGLEC10 signaling pathway is a potential target for cancer

immunotherapy, as suppressing immune responses may reduce inflammatory damage (63). CD47, a widely expressed transmembrane protein, acts as a "don't eat me" signal by interacting with SIRPa on macrophages to inhibit phagocytosis. Casey et al. found that MYC regulates CD47 expression, with its high expression suppressing anti-tumor immune responses (64). HAVCR2 (TIM-3), an innate and adaptive immune checkpoint molecule, is associated with T cell exhaustion when highly expressed. Pan-cancer analyses have shown that elevated HAVCR2 expression correlates with immune infiltration and checkpoint genes, potentially serving as a key factor in immunosuppression (65). Based on our findings, we propose that the high expression of these immune checkpoint genes may suppress immune cell activation, reduce inflammation, maintain immune balance, and prevent excessive tissue damage. This mechanism likely contributes to immune homeostasis in the later stages of sepsis. Cell communication analysis indicated enhanced IL-1 signaling and suppressed HLA-DRB1-CD4 signaling, suggesting impaired antigen presentation that may further weaken T cell function. IL-1 receptor antagonists, such as anakinra, may mitigate renal inflammation by blocking this pathway. Metabolic pathway analysis revealed upregulated biotin and lipoic acid metabolism, indicating metabolic reprogramming that supports the pro-inflammatory functions of neutrophils, offering new avenues for metabolic interventions, such as biotin supplementation.



The rat cecal ligation and puncture model and human peripheral blood validation experiments bolstered the reliability of our bioinformatics findings. The cecal ligation and puncture model demonstrated that elevated PADI4 expression (P < 0.001) was associated with enhanced NETosis (increased citH3 signaling), while PADI4 knockdown significantly alleviated acute kidney

injury pathology (P < 0.01), supporting PADI4 as a central driver of renal damage by pro-inflammatory neutrophils (45). In human peripheral blood, the high expression of PADI4, CASP4, CR1, and MAPK14 (P < 0.05) was consistent with bulk RNA sequencing results, with ROC analysis (AUC 0.67-0.97) further validating their diagnostic potential.

A notable limitation of this study is the reliance on general sepsis datasets (GSE175453 and GSE167363), which primarily capture systemic immune responses rather than kidney-specific pathology, and the use of the CLP model, which induces systemic sepsis but is not specific to SAKI. The absence of SAKI-specific clinical annotations in the datasets, such as KDIGO-based diagnostic criteria (e.g., serum creatinine or urine output), and the lack of quantitative kidney injury biomarkers (e.g., BUN, CR, NGAL, KIM-1) in the CLP model, limit direct attribution of neutrophil heterogeneity and hub gene effects to SAKI. Instead, our findings elucidate sepsis-induced immune dysregulation, particularly neutrophil-driven mechanisms, that may contribute to organ dysfunction including SAKI. Future studies utilizing SAKIspecific cohorts with detailed clinical data or SAKI-specific models (e.g., urosepsis models) with biomarker quantification could validate and extend these findings to establish direct links with kidney injury.

Despite significant progress, this study has limitations. Public datasets (GSE175453, GSE167363) and the cecal ligation and puncture model primarily reflect general sepsis mechanisms, lacking urosepsis-specific data and models, which limits direct insights into urinary tract infection-induced inflammation. The small sample size of human peripheral blood (n=5) may affect statistical robustness. Experimental validation focused on PADI4, and the roles of other genes, such as CASP4, require further exploration.

For requirements for a specific article type please refer to the Article Types on any Frontiers journal page. Please also refer to Author Guidelines for further information on how to organize your manuscript in the required sections or their equivalents for your field.

Data availability statement

The original contributions presented in the study are included in the article/Supplementary Material. Further inquiries can be directed to the corresponding author.

Ethics statement

The studies involving humans were approved by the Ethics Committee of Zhuzhou Hospital Affiliated to Xiangya School of Medicine, Central South University (Approval No: 2020175-01). The studies were conducted in accordance with the local legislation and institutional requirements. The participants provided their written informed consent to participate in this study. The animal study was approved by Institutional Animal Care and Use Committee of The Second Xiangya Hospital, Central South

University (Approval No: 2022711). The study was conducted in accordance with the local legislation and institutional requirements.

Author contributions

TC: Writing – original draft, Visualization, Validation, Formal Analysis. YX: Writing – review & editing. ZL: Writing – review & editing. ZZ: Writing – review & editing. ZZ: Writing – review & editing. WH: Conceptualization, Supervision, Writing – review & editing, Data curation, Formal Analysis, Methodology.

Funding

The author(s) declare financial support was received for the research and/or publication of this article. Hunan Provincial Natural Science Foundation of China(2023JJ41065). Hunan Provincial Natural Science Foundation of China(2025JJ70038).

Conflict of interest

The authors declare that the research was conducted in the absence of any commercial or financial relationships that could be construed as a potential conflict of interest.

Generative Al statement

The author(s) declare that no Generative AI was used in the creation of this manuscript.

Any alternative text (alt text) provided alongside figures in this article has been generated by Frontiers with the support of artificial intelligence and reasonable efforts have been made to ensure accuracy, including review by the authors wherever possible. If you identify any issues, please contact us.

Publisher's note

All claims expressed in this article are solely those of the authors and do not necessarily represent those of their affiliated organizations, or those of the publisher, the editors and the reviewers. Any product that may be evaluated in this article, or claim that may be made by its manufacturer, is not guaranteed or endorsed by the publisher.

Supplementary material

The Supplementary Material for this article can be found online at: https://www.frontiersin.org/articles/10.3389/fimmu.2025. 1637692/full#supplementary-material

References

- 1. Cecconi M, Evans L, Levy M, Rhodes A. Sepsis and septic shock. *Lancet*. (2018) 392:75–87. doi: 10.1016/S0140-6736(18)30696-2
- 2. Poston JT, Koyner JL. Sepsis associated acute kidney injury. BMJ. (2019) 364: k4891. doi: $10.1136/\mathrm{bmj.k4891}$
- 3. Bagheri Y, Ahmadian E, Hejazian SM, Raeesi M, Zununi Vahed S, Ardalan M. The effect of fingolimod on renal ischemia/reperfusion injury in a rat model. *Curr Mol Pharmacol.* (2024) 17:e250823220363. doi: 10.2174/1874467217666230825113406
- 4. Bellomo R, Kellum JA, Ronco C, Wald R, Martensson J, Maiden M, et al. Acute kidney injury in sepsis. *Intensive Care Med.* (2017) 43:816–28. doi: 10.1007/s00134-017-4755-7
- 5. Kellum JA, Romagnani P, Ashuntantang G, Ronco C, Zarbock A, Anders HJ. Acute kidney injury. *Nat Rev Dis Primers*. (2021) 7:52. doi: 10.1038/s41572-021-00284-z
- 6. Peerapornratana S, Manrique-Caballero CL, Gomez H, Kellum JA. Acute kidney injury from sepsis: current concepts, epidemiology, pathophysiology, prevention and treatment. *Kidney Int.* (2019) 96:1083–99. doi: 10.1016/j.kint.2019.05.026
- 7. Scapini P, Cassatella MA. Social networking of human neutrophils within the immune system. *Blood.* (2014) 124:710–9. doi: 10.1182/blood-2014-03-453217
- 8. Hong Y, Chen L, Sun J, Xing L, Yang Y, Jin X, et al. Single-cell transcriptome profiling reveals heterogeneous neutrophils with prognostic values in sepsis. *iScience*. (2022) 25:105301. doi: 10.1016/j.isci.2022.105301
- 9. Xu P, Tao Z, Zhang C. Integrated multi-omics and artificial intelligence to explore new neutrophils clusters and potential biomarkers in sepsis with experimental validation. *Front Immunol.* (2024) 151377817. doi: 10.3389/fimmu.2024.1377817
- 10. Mangiola S, Doyle MA, Papenfuss AT. Interfacing Seurat with the R tidy universe. *Bioinformatics*. (2021) 37:4100–7. doi: 10.1093/bioinformatics/btab404
- 11. Korsunsky I, Millard N, Fan J, Slowikowski K, Zhang F, Wei K, et al. Fast, sensitive and accurate integration of single-cell data with Harmony. *Nat Methods*. (2019) 16:1289–96. doi: 10.1038/s41592-019-0619-0
- 12. Trapnell C, Cacchiarelli D, Grimsby J, Pokharel P, Li S, Morse M, et al. The dynamics and regulators of cell fate decisions are revealed by pseudotemporal ordering of single cells. *Nat Biotechnol.* (2014) 32:381–6. doi: 10.1038/nbt.2859
- 13. Kang Z, Peng C, Cheng J, Cheng Q. LogDet rank minimization with application to subspace clustering. *Comput Intell Neurosci.* (2015) 2015:824289. doi: 10.1155/2015/824289
- 14. Yu G, Wang L-G, Han Y, He Q-Y. clusterProfiler: an R package for comparing biological themes among gene clusters. *OMICS: A J Integr Biol.* (2012) 16:284–7. doi: 10.1089/omi.2011.0118
- 15. Jin S, Guerrero-Juarez CF, Zhang L, Chang I, Ramos R, Kuan CH, et al. Inference and analysis of cell-cell communication using CellChat. *Nat Commun.* (2021) 12:1088. doi: 10.1038/s41467-021-21246-9
- 16. Wang R, Zhang P, Wang J, Ma L, E W, Suo S, et al. Construction of a cross-species cell landscape at single-cell level. *Nucleic Acids Res.* (2022) 51:501–16. doi: 10.1093/nar/gkac633
- 17. Wang H, Zhu S, Zhou Z, Wang Z, Zhuang W, Xue D, et al. TR4 worsen urosepsis by regulating GSDMD. Eur J Med Res. (2024) 29:151. doi: 10.1186/s40001-024-01742-6
- 18. Shao Q, Chen D, Chen S, Ru X, Ye Q. Escherichia coli infection sepsis: an analysis of specifically expressed genes and clinical indicators. *Diagnostics (Basel)*. (2023) 13:3542. doi: 10.3390/diagnostics13233542
- 19. Johnson JR, Porter S, Johnston B, Kuskowski MA, Spurbeck RR, Mobley HL, et al. Host characteristics and bacterial traits predict experimental virulence for Escherichia coli bloodstream isolates from patients with urosepsis. *Open Forum Infect Dis.* (2015) 2:ofv083. doi: 10.1093/ofid/ofv083
- 20. Davis S, Meltzer PS. GEOquery: a bridge between the gene expression omnibus (GEO) and BioConductor. *Bioinformatics*. (2007) 23:1846–7. doi: 10.1093/bioinformatics/btm254
- 21. Irizarry RA, Bolstad BM, Collin F, Cope LM, Hobbs B, Speed TP. Summaries of Affymetrix GeneChip probe level data. *Nucleic Acids Res.* (2003) 31:e15–e. doi: 10.1093/nar/gng015
- 22. Sijie W, Caipeng X, Huihui H, Pei Y, Haijing Z, Yuqiang W, et al. iTRAQ-based proteomic analysis unveils NCAM1 as a novel regulator in doxorubicin-induced cardiotoxicity and DT-010-exerted cardioprotection. *Curr Pharm Anal.* (2024) 20:966–77. doi: 10.2174/0115734129331758241022113026
- 23. Robin X, Turck N, Hainard A, Tiberti N, Lisacek F, Sanchez J-C, et al. pROC: an open-source package for R and S+ to analyze and compare ROC curves. *BMC Bioinf*. (2011) 12:77. doi: 10.1186/1471-2105-12-77
- 24. Aran D, Hu Z, Butte AJ. xCell: digitally portraying the tissue cellular heterogeneity landscape. *Genome Biol.* (2017) 18:220. doi: 10.1186/s13059-017-1349-1
- 25. Revelle WR. psych: Procedures for personality and psychological research. (2017). Available online at: https://www.scholars.northwestern.edu/en/publications/psych-procedures-for-personality-and-psychological-research.
- 26. Cao Z, Zhao M, Sun H, Hu L, Chen Y, Fan Z. Roles of mitochondria in neutrophils. Front Immunol. (2022) 13:934444. doi: 10.3389/fimmu.2022.934444

- 27. Peng S, Gao J, Stojkov D, Yousefi S, Simon HU. Established and emerging roles for mitochondria in neutrophils. *Immunol Rev.* (2023) 314:413–26. doi: 10.1111/jmr.13158
- 28. Hewitson JP, West KA, James KR, Rani GF, Dey N, Romano A, et al. Malat1 suppresses immunity to infection through promoting expression of Maf and IL-10 in Th cells. *J Immunol.* (2020) 204:2949–60. doi: 10.4049/jimmunol.1900940
- 29. Overbeek SA, Henricks PA, Srienc AI, Koelink PJ, de Kruijf P, Lim HD, et al. Nacetylated Proline-Glycine-Proline induced G-protein dependent chemotaxis of neutrophils is independent of CXCL8 release. *Eur J Pharmacol.* (2011) 668:428–34. doi: 10.1016/j.ejphar.2011.03.022
- 30. OuYang X, Liu P, Zheng Y, Jiang H, Lv Q, Huang W, et al. TRIM32 reduced the recruitment of innate immune cells and the killing capacity of Listeria monocytogenes by inhibiting secretion of chemokines. *Gut Pathog.* (2023) 15:32. doi: 10.1186/s13099-023-00558-9
- 31. Hwaiz R, Rahman M, Syk I, Zhang E, Thorlacius H. Rac1-dependent secretion of platelet-derived CCL5 regulates neutrophil recruitment via activation of alveolar macrophages in septic lung injury. *J Leukoc Biol.* (2015) 97:975–84. doi: 10.1189/ilb.4A1214-603R
- 32. Ha H, Bensman T, Ho H, Beringer PM, Neamati N. A novel phenylcyclohex-1-enecarbothioamide derivative inhibits CXCL8-mediated chemotaxis through selective regulation of CXCR2-mediated signalling. *Br J Pharmacol.* (2014) 171:1551–65. doi: 10.1111/bph.12547
- 33. Fan W, Wang C, Xu K, Liang H, Chi Q. Ccl5(+) Macrophages drive proinflammatory responses and neutrophil recruitment in sepsis-associated acute kidney injury. *Int Immunopharmacol.* (2024) 143:113339. doi: 10.1016/j.intimp.2024.113339
- 34. Suzuki K, Tsuchiya M, Yoshida S, Ogawa K, Chen W, Kanzaki M, et al. Tissue accumulation of neutrophil extracellular traps mediates muscle hyperalgesia in a mouse model. *Sci Rep.* (2022) 12:4136. doi: 10.1038/s41598-022-07916-8
- 35. Xiao Z, Visentin GP, Dayananda KM, Neelamegham S. Immune complexes formed following the binding of anti-platelet factor 4 (CXCL4) antibodies to CXCL4 stimulate human neutrophil activation and cell adhesion. *Blood.* (2008) 112:1091–100. doi: 10.1182/blood-2008-04-153288
- 36. Pignatti P, Moscato G, Casarini S, Delmastro M, Poppa M, Brunetti G, et al. Downmodulation of CXCL8/IL-8 receptors on neutrophils after recruitment in the airways. *J Allergy Clin Immunol.* (2005) 115:88–94. doi: 10.1016/j.jaci.2004.08.048
- 37. Majewska E, Wittek N, Rysz J, Baj Z. The influence of uremic high cystatin C concentration on neutrophil apoptosis and selected neutrophil functions isolated from healthy subjects. *Med Sci Monit.* (2012) 18:CR667–73. doi: 10.12659/MSM.883545
- 38. Niu X, Wang B. A network medical framework based on inflammatory genes to identify drug candidates for abdominal aortic aneurysms. *Curr Mol Pharmacol.* (2024) 17:e170523216998. doi: 10.2174/1874467217666230517104426
- 39. Peng Z, Fang C, Tong Z, Rao Q, Ren Z, Hu K. Crosstalk between cancer-associated fibroblasts and myeloid cells shapes the heterogeneous microenvironment of gastric cancer. *Curr Genomics*. (2024) 25:390–411. doi: 10.2174/0113892029300608240531111743
- 40. Yan S, Han Z, Wang T, Wang A, Liu F, Yu S, et al. Exploring the immune-related molecular mechanisms underlying the comorbidity of temporal lobe epilepsy and major depressive disorder through integrated data set analysis. *Curr Mol Pharmacol.* (2024) 17:e18761429380394. doi: 10.2174/0118761429380394250217093030
- 41. Salazar-Gonzalez H, Zepeda-Hernandez A, Melo Z, Saavedra-Mayorga DE, Echavarria R. Neutrophil extracellular traps in the establishment and progression of renal diseases. *Med (Kaunas)*. (2019) 55:431. doi: 10.3390/medicina55080431
- 42. Cuthbert GL, Daujat S, Snowden AW, Erdjument-Bromage H, Hagiwara T, Yamada M, et al. Histone deimination antagonizes arginine methylation. *Cell.* (2004) 118:545–53. doi: 10.1016/j.cell.2004.08.020
- 43. Hagiwara T, Hidaka Y, Yamada M. Deimination of histone H2A and H4 at arginine 3 in HL-60 granulocytes. *Biochemistry*. (2005) 44:5827–34. doi: 10.1021/bi047505c
- 44. Thiam HR, Wong SL, Wagner DD, Waterman CM. Cellular mechanisms of NETosis. *Annu Rev Cell Dev Biol.* (2020) 36:191–218. doi: 10.1146/annurev-cellbio-020520-111016
- 45. Wong SL, Wagner DD. Peptidylarginine deiminase 4: a nuclear button triggering neutrophil extracellular traps in inflammatory diseases and aging. FASEB J. (2018) 32: fj201800691R. doi: 10.1096/fj.201800691R
- 46. Lewis HD, Liddle J, Coote JE, Atkinson SJ, Barker MD, Bax BD, et al. Inhibition of PAD4 activity is sufficient to disrupt mouse and human NET formation. *Nat Chem Biol.* (2015) 11:189–91. doi: 10.1038/nchembio.1735
- 47. Wu SY, Weng CL, Jheng MJ, Kan HW, Hsieh ST, Liu FT, et al. Candida albicans triggers NADPH oxidase-independent neutrophil extracellular traps through dectin-2. *PloS Pathog.* (2019) 15:e1008096. doi: 10.1371/journal.ppat.1008096
- 48. Ham A, Rabadi M, Kim M, Brown KM, Ma Z, D'Agati V, et al. Peptidyl arginine deiminase-4 activation exacerbates kidney ischemia-reperfusion injury. *Am J Physiol Renal Physiol.* (2014) 307:F1052–62. doi: 10.1152/ajprenal.00243.2014

49. Nian W, Tao W, Zhang H. Review of research progress in sepsis-associated acute kidney injury. Front Mol Biosci. (2025) 12:1603392. doi: 10.3389/fmolb.2025.1603392

- 50. Du M, Yang I, Gu J, Wu J, Ma Y, Wang T. Inhibition of peptidyl arginine deiminase-4 prevents renal ischemia-reperfusion-induced remote lung injury. *Mediators Inflamm.* (2020) 2020:1724206. doi: 10.1155/2020/1724206
- 51. Shi J, Zhao Y, Wang Y, Gao W, Ding J, Li P, et al. Inflammatory caspases are innate immune receptors for intracellular LPS. *Nature*. (2014) 514:187–92. doi: 10.1038/nature13683
- 52. Smith AP, Creagh EM. Caspase-4 and -5 biology in the pathogenesis of inflammatory bowel disease. *Front Pharmacol.* (2022) 13:919567. doi: 10.3389/fphar.2022.919567
- 53. Hardy MP, Mansour M, Rowe T, Wymann S. The molecular mechanisms of complement receptor 1-it is complicated. *Biomolecules*. (2023) 13:1522. doi: 10.3390/biom13101522
- 54. Birmingham DJ, Hebert LA. CR1 and CR1-like: the primate immune adherence receptors. *Immunol Rev.* (2001) 180:100-11. doi: 10.1034/j.1600-065X.2001.1800109.x
- 55. Khera R, Das N. Complement Receptor 1: disease associations and therapeutic implications. *Mol Immunol.* (2009) 46:761–72. doi: 10.1016/j.molimm.2008.09.026
- 56. Madkour MM, Anbar HS, El-Gamal MI. Current status and future prospects of p38alpha/MAPK14 kinase and its inhibitors. *Eur J Med Chem.* (2021) 213:113216. doi: 10.1016/j.ejmech.2021.113216
- 57. Wang J, Liu Y, Guo Y, Liu C, Yang Y, Fan X, et al. Function and inhibition of P38 MAP kinase signaling: Targeting multiple inflammation diseases. *Biochem Pharmacol.* (2024) 220:115973. doi: 10.1016/j.bcp.2023.115973

- 58. Qi X, Yu Y, Sun R, Huang J, Liu L, Yang Y, et al. Identification and characterization of neutrophil heterogeneity in sepsis. *Crit Care.* (2021) 25:50. doi: 10.1186/s13054-021-03481-0
- 59. Hotchkiss RS, Monneret G, Payen D. Immunosuppression in sepsis: a novel understanding of the disorder and a new therapeutic approach. *Lancet Infect Dis.* (2013) 13:260–8. doi: 10.1016/S1473-3099(13)70001-X
- 60. Young JS, Heffernan DS, Chung CS, Kettenmann ML, Young WA, Guillen VS, et al. Effect of PD-1: PD-L1 in invariant natural killer T-cell emigration and chemotaxis following sepsis. *Shock.* (2016) 45:534–9. doi: 10.1097/SHK.00000000000000553
- 61. van Vught LA, Wiewel MA, Hoogendijk AJ, Frencken JF, Scicluna BP, Klein Klouwenberg PMC, et al. The host response in patients with sepsis developing intensive care unit-acquired secondary infections. *Am J Respir Crit Care Med.* (2017) 196:458–70. doi: 10.1164/rccm.201606-1225OC
- 62. Barkal AA, Brewer RE, Markovic M, Kowarsky M, Barkal SA, Zaro BW, et al. CD24 signalling through macrophage Siglec-10 is a target for cancer immunotherapy. *Nature*. (2019) 572:392–6. doi: 10.1038/s41586-019-1456-0
- 63. Li X, Tian W, Jiang Z, Song Y, Leng X, Yu J. Targeting CD24/Siglec-10 signal pathway for cancer immunotherapy: recent advances and future directions. *Cancer Immunol Immunother.* (2024) 73:31. doi: 10.1007/s00262-023-03606-0
- 64. Casey SC, Tong L, Li Y, Do R, Walz S, Fitzgerald KN, et al. MYC regulates the antitumor immune response through CD47 and PD-L1. *Science*. (2016) 352:227–31. doi: 10.1126/science.aac9935
- 65. Li H, Yang D, Hao M, Liu H. Differential expression of HAVCR2 gene in pancancer: A potential biomarker for survival and immunotherapy. *Front Genet.* (2022) 13:972664. doi: 10.3389/fgene.2022.972664